

Helicity transfer in compressible turbulent flows

Zheng Yan , Junfeng Wu , and Zhu Lei 

Institute of Applied Physics and Computational Mathematics, Beijing 100094, China

Jianchun Wang 

Department of Mechanics and Aerospace Engineering, Southern University of Science and Technology, Shenzhen, Guangdong 518055, China

Lifeng Wang *

*Institute of Applied Physics and Computational Mathematics, Beijing 100094, China
and Center for Applied Physics and Technology, HEDPS, Peking University, Beijing 100871, China*

Xinliang Li 

*LHD, Institute of Mechanics, Chinese Academy of Sciences, Beijing 100190, China
and School of Engineering Science, University of Chinese Academy of Sciences, Beijing 100049, China*

Changping Yu †

LHD, Institute of Mechanics, Chinese Academy of Sciences, Beijing 100190, China



(Received 3 July 2024; accepted 21 August 2024; published 4 September 2024)

The dual-channel characteristics of large-scale helicity transfer in compressible turbulent flows, including subgrid-scale (SGS) and viscosity terms, are investigated. After selecting a suitable definition for large-scale helicity, we confirm the existence of the dual channel of SGS and viscosity terms of large-scale helicity governing equations and theoretically prove that no dual pressure term channel exists. The second channel of the SGS and viscosity terms also consists of two terms, which originate from the rotation of the SGS stress and the baroclinic of the velocity and density gradients, respectively. The identical relationship of the ensemble averages of the dual channel of SGS and viscosity terms can be theoretically and numerically confirmed, whereas their second channel which is associated with shocklets is more intermittent. For the SGS term, the compression regions are dominant in contrast to the expansion regions, and the strain regions are dominant in contrast to the rotation regions in the inertial scale range. The viscous dissipation mechanism of large-scale helicity differs from that of large-scale kinetic energy. It is dominated by the first channel on the inside of the vortex structure and by the second channel on the outside. The further decompositions of the second channel of the SGS and viscosity terms provide a possible mechanism for the inverse helicity transfer. This means that expansion motions promote inverse helicity transfer through the second terms of their second channels.

DOI: [10.1103/PhysRevFluids.9.094603](https://doi.org/10.1103/PhysRevFluids.9.094603)

*Contact author: wang_lifeng@iapcm.ac.cn

†Contact author: cpyu@imech.ac.cn

I. INTRODUCTION

Helicity is defined as the integral of velocity $\mathbf{u}(\mathbf{x}, t)$ and vorticity $\boldsymbol{\omega}(\mathbf{x}, t)$ over volume, and it is expressed as

$$H(t) = \frac{1}{V} \int_V \mathbf{u}(\mathbf{x}, t) \cdot \boldsymbol{\omega}(\mathbf{x}, t) \, d\mathbf{x}. \quad (1)$$

The integrand $h(t) = \mathbf{u}(\mathbf{x}, t) \cdot \boldsymbol{\omega}(\mathbf{x}, t)$ is called the helicity density. Consistent with the Helmholtz and Kelvin theorems, if we assume that the flows are inviscid and barotropic, the helicity-governing equation is reduced to

$$\partial_t(\mathbf{u} \cdot \boldsymbol{\omega}) + \nabla \cdot ((\mathbf{u} \cdot \boldsymbol{\omega})\mathbf{u} + [p(\rho) - \frac{1}{2}|\mathbf{u}|^2]\boldsymbol{\omega}) = 0, \quad (2)$$

where $p(\rho)$ is the pressure in the case of barotropic fluid [1–3]. When an ensemble average of the above equation is used, the conservation law of helicity is present [4,5]. Nevertheless, the inviscid and barotropic conditions cannot be satisfied in practical compressible turbulent flows [6]. However, the helicity cascade process is still regarded as statistically conservative at the inertial subrange. The main reason lies in the fact that viscosity works only on small scales and that pressure works only on large scales statistically [7]. Relative to kinetic energy, helicity is pseudoscalar, which means that its sign depends on the selected reference frame. Helicity topologically measures the twisting, linking, and writhing of vortex lines even in a viscous flow [8–11].

Over the past few decades, scholars have had mixed views on the effects of helicity on the statistical properties of turbulent flows. Some insist that helicity is a passive scalar and is not associated with the energy spectra distribution [12–14]. In contrast, others believe that helicity can weaken the nonlinearity strength of Navier-Stokes equations (NSEs) [15–17], the viscosity dissipation rate of kinetic energy [18], the kinetic energy cascade process [19], kinetic energy transfer into internal energy [7], and the decay rate of kinetic energy in rotating flows [20] and can promote the inverse energy cascade process [21–26]. These helicity effects provide some theoretical suggestions for developing suitable control methods for engineering flows, such as enhancing engine efficiency, controlling rainfall intensity, and decreasing aircraft drag.

The study of helicity provides some new perspectives for natural and engineering flows. Supercell formation and violent storms in atmospheric flows can be predicted by measuring helicity [27,28]. The conservation of magnetic helicity promotes the understanding of the Earth’s magnetosphere and solar corona [29,30] and the development of tokamak reactors. The existence of helicity in a jet-stirred tubular reactor leads to a higher turbulent mixing efficiency [31]. The study of helicity can reveal associated flow structures beneficial to scalar transport in wall turbulence [32]. The Taylor-Görtler vortices in turbulent boundary layers can also be considered helical structures with high helicity [33,34], providing a possible explanation for the high heat flux in hypersonic vehicles [35,36].

There exists a joint turbulent cascade of kinetic energy and helicity in three-dimensional turbulent flows, which can be derived from Euler’s equations [12,37–39]. Many efforts have been devoted to the study of energy cascades in incompressible and compressible turbulent flows [25,40–43], and some methodologies can be extended to investigations of helicity cascades. Ditlevsen and Giuliani [44] confirmed the existence of the helicity dissipation scale, which is analogous to the Kolmogorov scale. Kurien *et al.* [45] proposed a helicity transfer timescale by using phenomenological arguments. Chen *et al.* [39] compared the intermittency discrepancy of energy and helicity fluxes using the refined similarity hypothesis. Eyink [40] proposed a multiscale gradient expansion method for the subgrid-scale (SGS) stress tensor and obtained the approximate energy and helicity flux forms. Biferale *et al.* [22] and Sahoo *et al.* [23,46] changed the nature of nonlinear terms of NSEs by modifying the initial flow field into a single chirality and proposed a possible mechanism for the inverse energy cascade in three-dimensional turbulent flows. Sahoo *et al.* [47] studied the scaling properties of high-order structure functions of velocity and vorticity increments. In addition, the

helical wave decomposition method was also employed to investigate the spectral properties of energy and helicity with different chirality [24,38,48–50].

The presence of shock in compressible turbulent flows leads to a great challenge for the helicity conservation law and other statistical properties of helicity transfer [3]. In addition, the variable-density effect, couplings between velocity fields and thermodynamic parameters, and couplings among vorticity and acoustic and entropy modes present only in compressible turbulent flows lead to greater difficulty in helicity investigations. The coupling of the solenoidal and compressible modes leads to a theoretical challenge for exploring the intrinsic mechanism of compressible turbulent flows [51]. In compressible flows, the role of viscosity is more complex, and compressibility plays an essential role in helicity generation [3,52]. Given the existence of large-scale helical structures, a bridge should exist to transfer helicity from small scales to large scales [53,54]. Several previous attempts were made by the authors to address the issues of helicity transfer in compressible turbulent flows, including study of the effects of helicity on the energy cascade process [19], the effect of pressure on the helicity cascade at relatively large scales [7], and cross-chirality transfer of kinetic energy and helicity [55]. Our previous work on dual-channel helicity cascade theory in incompressible turbulent flows [56] led to the question of whether the dual helicity cascade channel exists in compressible turbulent flows. To address this issue, first, we need to choose a suitable definition of large-scale helicity to satisfy the conservation law and eliminate pressure and viscosity. Second, the expressions of the dual-channel helicity cascade should be derived, and a contrastive study of the differences between incompressible turbulent flows and compressible turbulent flows should be performed. Third, in addition to SGS terms, the question of whether the dual-channel methodology applies to pressure and viscosity terms should be answered.

These problems motivate us to conduct a detailed investigation of large-scale helicity transfer in compressible turbulent flows. The rest of the paper is organized as follows. In Sec. II we present the details of direct numerical simulations (DNS) of compressible helical turbulent flows. In Sec. III we derive the governing equation of large-scale helicity in compressible turbulent flows and confirm the existence of dual channels of SGS and viscosity terms in helicity transfer. Then in Sec. IV we investigate the statistical properties of the two channels of the SGS and viscosity terms under the effects of compression, expansion, strain, and rotation. In Sec. V we summarize the major conclusions and discuss the findings of the study.

II. DNS OF COMPRESSIBLE HELICAL TURBULENCE

Some reference variables are selected to normalize the physical variables present in the governing equations: the reference density ρ_f , velocity U_f , pressure $p_f = \rho_f U_f^2$, temperature T_f , length L_f , viscosity μ_f , thermal conductivity κ_f , and energy per unit volume $\rho_f U_f^2$. The dimensionless parameters involved include the Reynolds number $\text{Re} \equiv \rho_f U_f L_f / \mu_f$, Mach number $M \equiv U_f / c_f$, and Prandtl number $\text{Pr} \equiv \mu_f C_p / \kappa_f$, which is set to 0.7. $c_f \equiv \sqrt{\gamma R T_f}$ is the speed of sound, where $\gamma \equiv C_p / C_v$ is the heat capacity ratio, which is set to 1.4 in our numerical simulation; C_p is the specific heat at constant pressure; C_v is the specific heat at constant volume; and $\alpha \equiv \text{PrRe}(\gamma - 1)M^2$ [55,57,58].

The dimensionless NSEs for three-dimensional compressible helical turbulence of ideal gas are

$$\frac{\partial \rho}{\partial t} + \frac{\partial(\rho u_j)}{\partial x_j} = 0, \quad (3a)$$

$$\frac{\partial(\rho u_i)}{\partial t} + \frac{\partial(\rho u_i u_j)}{\partial x_j} = -\frac{\partial p}{\partial x_i} + \frac{1}{\text{Re}} \frac{\partial \sigma_{ij}}{\partial x_j} + F_i, \quad (3b)$$

$$\frac{\partial \mathcal{E}}{\partial t} + \frac{\partial[(\mathcal{E} + p)u_j]}{\partial x_j} = \frac{1}{\alpha} \frac{\partial}{\partial x_j} \left(\kappa \frac{\partial T}{\partial x_j} \right) + \frac{1}{\text{Re}} \frac{\partial(\sigma_{ij} u_i)}{\partial x_j} - \Lambda + F_j u_j, \quad (3c)$$

$$p = \frac{\rho T}{\gamma M^2}. \quad (3d)$$

where ρ is the density, \mathbf{u} is the velocity, p is the pressure, T is the temperature, Λ is a cooling function for sustaining a steady state statistically [57], and \mathbf{F} is the large-scale force composed of multiple parameters controlling kinetic energy and helicity. The multiple parameters include the energy input rates of the compressive and solenoidal components and the helicity input rate. Hence, the specific external force can be constructed as

$$F_i = \sqrt{\rho} \times (\pi_1 u_i^C + \pi_2 u_i^S + \pi_3 \omega_i), \quad (4)$$

where the superscripts C and S denote the compressible and solenoidal components of velocity, respectively, and π_1 , π_2 , and π_3 are three indeterminate dimensional parameters. The external force is fixed within the lowest two wave-number shells to avoid the pollution of external force on the statistical results at middle and small scales. Similar to our previous work [55], the injection rates of kinetic energy and helicity are fixed at 0.3 and -0.37 , respectively. To obtain highly compressible turbulent flows, the injection rate of the kinetic energy is divided equally into solenoidal and compressible modes. For more details, refer to our previous work [55].

In addition, the viscous stress is defined as

$$\sigma_{ij} = \mu \left(\frac{\partial u_i}{\partial x_j} + \frac{\partial u_j}{\partial x_i} \right) - \frac{2}{3} \mu \frac{\partial u_k}{\partial x_k} \delta_{ij}. \quad (5)$$

The total energy per unit volume \mathcal{E} is

$$\mathcal{E} = \frac{p}{\gamma - 1} + \frac{1}{2} \rho u_i u_i. \quad (6)$$

The viscosity coefficient μ and thermal conductivity coefficient κ are determined via the Sutherland law [59] for simplicity:

$$\mu = \frac{1.4042T^{1.5}}{T + 0.40417}, \quad \kappa = \frac{1.4042T^{1.5}}{T + 0.40417}. \quad (7)$$

The DNS of compressible helical turbulence in a cubic box with a length of 2π is carried out in the present study. To obtain high-fidelity numerical results to capture all the length scales of interest, the grid resolution is 2048^3 , and we adopt periodic boundary conditions in the x , y , and z directions. For more numerical setting details, refer to our previous work [55].

Some one-point statistical parameters are defined to describe the characteristics of the present compressible helical turbulence [60,61]. The integral length scale L_f is

$$L_f = \frac{3\pi}{2\langle u' \rangle^2} \int_0^\infty \frac{E^u(k)}{k} dk, \quad (8)$$

where $E^u(k)$ is the power spectrum of the velocity with $\int_0^\infty E^u(k) dk = \langle u^2 \rangle / 2$. The Taylor microscale λ is

$$\lambda = \frac{u'}{\langle [(\partial u_1 / \partial x_1)^2 + (\partial u_2 / \partial x_2)^2 + (\partial u_3 / \partial x_3)^2] / 3 \rangle^{1/2}}, \quad (9)$$

and the Kolmogorov length scale η is

$$\eta = [\langle \mu / \text{Re} \rho \rangle^3 / \epsilon]^{1/4}. \quad (10)$$

Here u' is the root mean square (rms) of velocity vector \mathbf{u} , which is defined as $u' = \sqrt{\langle u_1^2 + u_2^2 + u_3^2 \rangle / 3}$; $E(k)$ is the spectrum of kinetic energy per unit mass; ϵ is the ensemble-averaged viscous dissipation rate of kinetic energy per unit volume, which is defined as $\epsilon = \langle \sigma_{ij} S_{ij} / \text{Re} \rangle$; and the strain-rate tensor is $S_{ij} = (1/2)(\partial u_i / \partial x_j + \partial u_j / \partial x_i)$. Hence, the Taylor microscale Reynolds number Re_λ and the turbulent Mach number M_t are defined as

$$\text{Re}_\lambda = \frac{u' \lambda \langle \rho \rangle}{\langle \mu \rangle}, \quad M_t = M \frac{\sqrt{3} u'}{\sqrt{T}}. \quad (11)$$

TABLE I. Some characteristic parameters of the present numerical simulations. Δx is the mesh spacing, θ' is the rms of the velocity divergence, and ω' is the rms of the vorticity magnitude.

| Resolution | Re_λ | M_t | ϵ | δ | $k_{\max}\eta$ | $\eta/\Delta x$ | L_f/η | λ/η | τ_η | T_0 | θ' | ω' | S_3 |
|------------|--------------|-------|------------|----------|----------------|-----------------|------------|----------------|-------------|-------|-----------|-----------|--------|
| 2048^3 | 514 | 0.67 | 0.30 | -0.37 | 3.23 | 1.03 | 477 | 33.96 | 0.032 | 0.94 | 22.22 | 20.47 | -30.76 |

The mean viscous dissipation rate of helicity is $\delta = 4\langle S_{ij}R_{ij} - S_{ii}R_{jj}/3 \rangle$, and $R_{ij} = (1/2)[\partial(\omega_i/\rho)/\partial x_j + \partial(\omega_j/\rho)/\partial x_i]$. τ_η is the Kolmogorov time scale, which is defined as $\tau_\eta = ((\mu/\rho)/\epsilon)^{1/2}$. T_0 is the large-eddy turnover time, which is defined as $T_0 = L_f/u'$. The skewness of the velocity gradient S_3 is defined as

$$S_3 = \frac{[(\partial u_1/\partial x_1)^3 + (\partial u_2/\partial x_2)^3 + (\partial u_3/\partial x_3)^3]/3}{[(\partial u_1/\partial x_1)^2 + (\partial u_2/\partial x_2)^2 + (\partial u_3/\partial x_3)^2]/3^{3/2}}. \quad (12)$$

The characteristic parameters of the flow fields are listed in Table I. To obtain the stationary status of fully developed helical turbulent flows, the computational physical time exceeds five times the large-eddy turnover time. We show the three-dimensional shocklet structures represented by the local velocity divergence of the present mesh resolution in Fig. 1(a). Owing to strong compressibility, the shocklets are composed of large-scale sheet structures, and the expansion structures are randomly distributed on a small scale. The kinetic energy spectra under different mesh resolutions are shown in Fig. 1(b). The kinetic energy spectra satisfies $\int_0^\infty E(k) dk = \langle v^2 \rangle / 2$, with $\mathbf{v} = \sqrt{\rho} \mathbf{u}$. In contrast to our previous result [55], the present energy spectrum with a higher Reynolds number and a higher mesh resolution exhibits more small-scale structures, which is beneficial to our statistical analysis.

Before evaluating the compression or expansion effects, we need to investigate the scale distributions of the velocity divergence. The power spectrum of the velocity divergence θ is defined as $\int_0^\infty E^\theta(k) dk = \langle \theta^2 \rangle$. In Fig. 2(a) we show the power spectrum of the velocity divergence. The power spectrum density of the velocity divergence in Fig. 2(a) shows a slight amplitude discrepancy at the large and middle length scales, and it indicates the fluctuation of the velocity divergence at the middle length scales is still large. However, both the compression and expansion motions are involved in the power spectrum of the velocity divergence. To assess the compression and expansion motions separately, we present the probability distribution functions (PDF) of the velocity

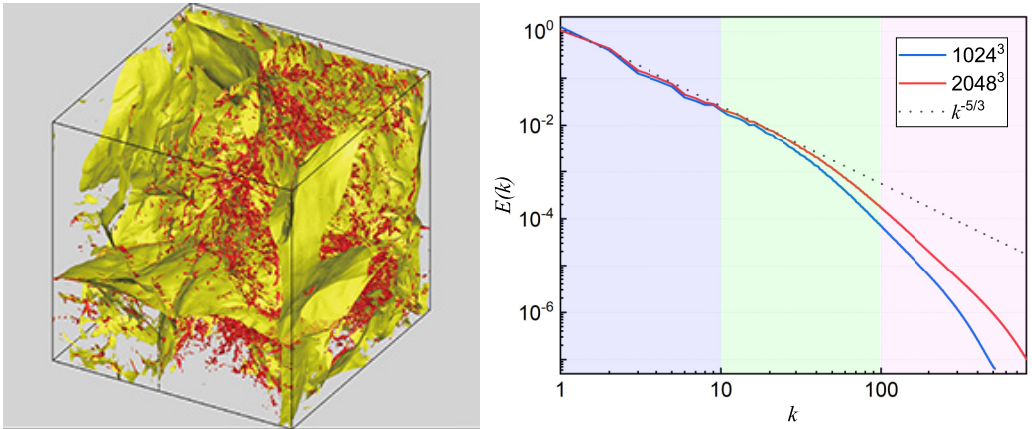


FIG. 1. (a) Isosurface of the velocity divergence, with threshold $\theta = -3\theta'$ rendered in yellow and $\theta = 0.5\theta'$ rendered in red. (b) Energy spectra of different mesh resolutions, and the energy spectrum of a mesh resolution with 1024^3 is obtained from our previous work [55].

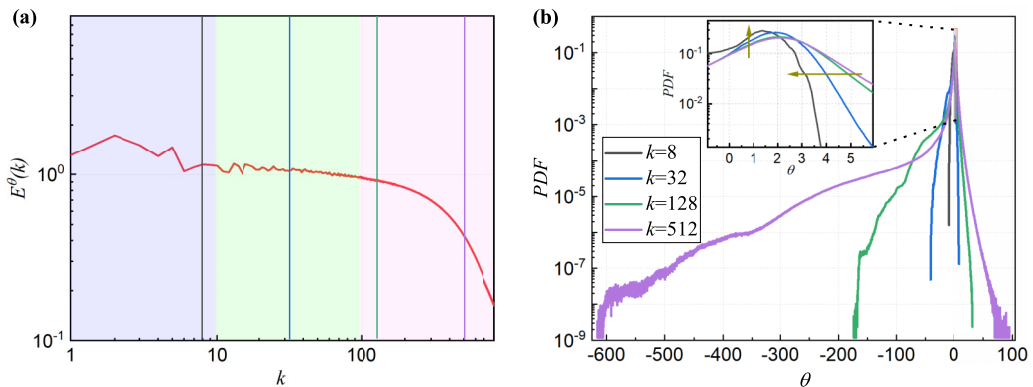


FIG. 2. (a) Power spectrum of the velocity divergence θ . (b) PDF of the velocity divergence at different length scales, where the line color corresponds to the length scales marked in (a). The inset shows the local enlarged PDF of the velocity divergence to highlight the distribution of the dilatation at different length scales.

divergence at the corresponding length scales in Fig. 2(b), which are marked in Fig. 2(a). The PDF of the velocity divergence indicates that the compression motion is dominant at all scales. With decreasing length scale, the degree of dominance increases, which is associated with the shocklet structures. For the PDF of the expansion motion shown in the inset of Fig. 2(b), weak expansion motions are more concentrated at the middle and large length scales. Hence, the compression and expansion motion degrees are high at the middle and small scales in our numerical simulations. This approach is beneficial for assessing the compression and expansion effects on SGS transfer at middle-length scales and on viscosity dissipation at small scales.

III. GOVERNING EQUATIONS OF LARGE-SCALE HELICITY IN COMPRESSIBLE TURBULENT FLOWS

Helicity is a scalar product of velocity and vorticity, and we define large-scale helicity as a scalar product of large-scale velocity and large-scale vorticity. However, two definitions of large-scale velocity exist for compressible flows. The first approach involves performing a filter operation on the velocity field, which is reflected as $\bar{\mathbf{u}}(\mathbf{x}) = \int d^3\mathbf{r} G_l(\mathbf{r}) \mathbf{u}(\mathbf{x} + \mathbf{r})$ [62]. The second definition is obtained through the Favre filter as $\tilde{\mathbf{u}}(\mathbf{x}) = \overline{\rho \mathbf{u}(\mathbf{x})} / \bar{\rho}$ [63]. The first definition is similar to that in incompressible flows, and the second definition involves nonconstant density effects, which are widely employed in compressible flows. In this section we derive the governing equations of large-scale helicity on the basis of the Favre-filtered large-scale velocity as $\tilde{H} = \tilde{\mathbf{u}} \cdot \tilde{\boldsymbol{\omega}}$, where $\tilde{\boldsymbol{\omega}} = \nabla \times \tilde{\mathbf{u}}$ [64] is the large-scale vorticity from the second definition. The governing equation of large-scale helicity based on the direct-filtered velocity $\bar{\mathbf{u}}$ and vorticity $\bar{\boldsymbol{\omega}} = \nabla \times \bar{\mathbf{u}}$ is derived and presented in Appendix A.

Performing a filter operation on Eq. (3b) without considering external force and dividing by $\bar{\rho}$, we can obtain the following large-scale velocity equation:

$$\frac{\partial \tilde{u}_i}{\partial t} + \tilde{u}_j \frac{\partial \tilde{u}_i}{\partial x_j} = -\frac{1}{\bar{\rho}} \frac{\partial \tilde{\tau}_{ij}}{\partial x_j} - \frac{1}{\bar{\rho}} \frac{\partial \bar{p}}{\partial x_i} + \frac{1}{\text{Re}} \frac{1}{\bar{\rho}} \frac{\partial \bar{\sigma}_{ij}}{\partial x_j}, \quad (13)$$

where the Favre-filtered subgrid-scale stress is $\tilde{\tau}_{ij} = \tilde{u}_i \tilde{u}_j - \tilde{u}_i \tilde{u}_j$. Performing a curl operation on Eq. (13), we can obtain the following Favre-filtered vorticity governing equation:

$$\frac{\partial \tilde{\omega}_i}{\partial t} + \tilde{u}_j \frac{\partial \tilde{\omega}_i}{\partial x_j} + \tilde{\omega}_i \tilde{\theta} = \tilde{\omega}_j \frac{\partial \tilde{u}_i}{\partial x_j} - \epsilon_{ijk} \frac{\partial}{\partial x_j} \left(\frac{1}{\bar{\rho}} \frac{\partial \tilde{\tau}_{kl}}{\partial x_l} \right) - \epsilon_{ijk} \frac{\partial}{\partial x_j} \left(\frac{1}{\bar{\rho}} \frac{\partial \bar{p}}{\partial x_k} \right) + \frac{1}{\text{Re}} \epsilon_{ijk} \frac{\partial}{\partial x_j} \left(\frac{1}{\bar{\rho}} \frac{\partial \bar{\sigma}_{kl}}{\partial x_l} \right). \quad (14)$$

Hence, combining Eqs. (13) and (14), we can obtain the following governing equations of large-scale helicity \tilde{H} with the Favre filter:

$$\frac{\partial \tilde{H}}{\partial t} + \frac{\partial \tilde{J}_j}{\partial x_j} = -\Pi_l^{H1} - \Pi_l^{H2} + \Phi_l + D_l, \quad (15)$$

where \tilde{J}_j is the spatial transport term, which is defined as

$$\begin{aligned} \tilde{J}_j = & \tilde{u}_j \tilde{H} - (1/2) \tilde{u}_i \tilde{u}_i \tilde{\omega}_j + \tilde{\omega}_i \tilde{\tau}_{ij} + \epsilon_{ikl} \frac{\partial \tilde{\rho} \tilde{\tau}_{lj}}{\partial x_k} \frac{\tilde{u}_i}{\tilde{\rho}} + \tilde{\rho} \tilde{\tau}_{ij} \epsilon_{ikl} \tilde{u}_k \frac{\partial}{\partial x_l} \left(\frac{1}{\tilde{\rho}} \right) \\ & + \tilde{p} \frac{\tilde{\omega}_j}{\tilde{\rho}} + \tilde{p} \epsilon_{jkl} \frac{\partial \tilde{\rho}}{\partial x_k} \frac{\tilde{u}_l}{\tilde{\rho}^2} - \tilde{\sigma}_{ij} \frac{\tilde{\omega}_i}{\tilde{\rho}} + \tilde{\sigma}_{ij} \epsilon_{ikl} \frac{\tilde{u}_k}{\tilde{\rho}^2} \frac{\partial \tilde{\rho}}{\partial x_l} - \frac{\tilde{u}_i}{\tilde{\rho}} \epsilon_{ikl} \frac{\partial \tilde{\sigma}_{lj}}{\partial x_k}. \end{aligned} \quad (16)$$

Here, according to the naming conventions in our previous work [56], Π_l^{H1} is the first channel originating from the advection term of the Favre-filtered velocity governing equation, and Π_l^{H2} is the second channel originating from the advection and vortex stretching terms of the Favre-filtered vorticity governing equation. They are defined as

$$\Pi_l^{H1} = -\tilde{\rho} \tilde{\tau}_{ij} \frac{\partial}{\partial x_j} \left(\frac{\tilde{\omega}_i}{\tilde{\rho}} \right), \quad (17)$$

$$\Pi_l^{H2} = \Pi_l^{H21} + \Pi_l^{H22}, \quad (18)$$

where

$$\Pi_l^{H21} = -\epsilon_{ikl} \frac{\partial \tilde{\rho} \tilde{\tau}_{lj}}{\partial x_k} \frac{\partial}{\partial x_j} \left(\frac{\tilde{u}_i}{\tilde{\rho}} \right), \quad \Pi_l^{H22} = -\tilde{\rho} \tilde{\tau}_{ij} \frac{\partial}{\partial x_j} \left[\epsilon_{ikl} \tilde{u}_k \frac{\partial}{\partial x_l} \left(\frac{1}{\tilde{\rho}} \right) \right]. \quad (19)$$

If we assume that the filtered density is a constant, Eq. (17) and the first term of Eq. (18) would recover to the first and second channels in incompressible flows [56]. Notably, the second term of the second channel depends on the density gradient, and it is present only in variable-density flows.

The tensor geometry determines the transfer efficiency between unresolved and resolved scales, in addition to the magnitudes of SGS stress and the strain rate for the energy cascade [65–68]. The tensor properties also lead to different transfer efficiencies, and a previous study proposed that the transfer efficiency of the two involved symmetric tensors is smaller than that of the two involved antisymmetric tensors for helicity cascades in incompressible turbulent flows [56]. The tensor involving the filtered vorticity and density in Eq. (17) can be decomposed into symmetric \tilde{R}_{ij} and antisymmetric components $\tilde{\Xi}_{ij}$ as follows:

$$\frac{\partial}{\partial x_j} \left(\frac{\tilde{\omega}_i}{\tilde{\rho}} \right) = \tilde{R}_{ij} + \tilde{\Xi}_{ij}, \quad (20)$$

where

$$\tilde{R}_{ij} = \frac{1}{2} \left[\frac{\partial}{\partial x_j} \left(\frac{\tilde{\omega}_i}{\tilde{\rho}} \right) + \frac{\partial}{\partial x_i} \left(\frac{\tilde{\omega}_j}{\tilde{\rho}} \right) \right], \quad \tilde{\Xi}_{ij} = \frac{1}{2} \left[\frac{\partial}{\partial x_j} \left(\frac{\tilde{\omega}_i}{\tilde{\rho}} \right) - \frac{\partial}{\partial x_i} \left(\frac{\tilde{\omega}_j}{\tilde{\rho}} \right) \right]. \quad (21)$$

The SGS stress tensor $\tilde{\rho} \tilde{\tau}_{ij}$ is symmetric, and its contraction with the antisymmetric component $\tilde{\Xi}_{ij}$ is zero. Hence, the first-channel helicity cascade involves only the contraction of two symmetric tensors. For the second term of the second-channel helicity cascade, the tensor involves the cross-product of the filtered velocity and density gradient, which is also decomposed into symmetric and antisymmetric components. Therefore, the tensor geometry of the second term of the second-channel helicity cascade is the same as that of the first channel.

The first term of the second-channel helicity cascade is more complex than that in incompressible form, and it is reflected in the rotation of the SGS stress tensor. We make a derivation to study the tensor properties in Appendix B and conclude that the first term of the second-channel helicity

cascade can be decomposed into a contraction of two antisymmetric tensors, similar to the incompressible form, and a component that results from compressibility.

The transfer efficiency of two symmetric tensors is greater than that of two antisymmetric tensors, and it can be explained as a simple geometry of antisymmetric tensors [56,65]. In compressible turbulent flows, the first channel of the helicity cascade can be considered the contraction of two symmetric tensors, whereas the second channel cannot be considered the contraction of two antisymmetric tensors. However, we infer that the transfer efficiency of the second channel of the helicity cascade is still greater than that of the first channel because the second channel involves the contraction of two antisymmetric tensors.

Φ_l refers to the pressure term, which is defined as

$$\Phi_l = \Phi_l^1 + \Phi_l^2, \quad \Phi_l^1 = \bar{\rho} \frac{\partial}{\partial x_j} \left(\frac{\tilde{\omega}_j}{\bar{\rho}} \right), \quad \Phi_l^2 = \bar{\rho} \frac{\partial}{\partial x_j} \left(\epsilon_{jkl} \frac{\partial \bar{\rho}}{\partial x_k} \frac{\tilde{u}_l}{\bar{\rho}^2} \right). \quad (22)$$

D_l denotes the viscous term, which is calculated as follows:

$$D_l = D_l^1 + D_l^2, \quad (23)$$

$$D_l^1 = -\bar{\sigma}_{ij} \frac{\partial}{\partial x_j} \left(\frac{\tilde{\omega}_i}{\bar{\rho}} \right), \quad D_l^2 = -\epsilon_{ikl} \frac{\partial \bar{\sigma}_{lj}}{\partial x_k} \frac{\partial}{\partial x_j} \left(\frac{\tilde{u}_i}{\bar{\rho}} \right) + \bar{\sigma}_{ij} \frac{\partial}{\partial x_j} \left(\epsilon_{ikl} \frac{\tilde{u}_k}{\bar{\rho}^2} \frac{\partial \bar{\rho}}{\partial x_l} \right). \quad (24)$$

The pressure term Φ_l and viscous term D_l on the right-hand side (r.h.s.) of Eq. (15) involve only large-scale flow fields, which can be resolved in large-eddy simulations (LES). The helicity flux terms Π_l^{H1} and Π_l^{H2} involve both large- and small-scale flow fields, which represent the interscale transfer of helicity in compressible flows. Hence, the form of the Favre-filtered helicity \tilde{H} could recapitulate the conservative characteristic of the helicity cascade in compressible flows, eliminating the pressure and viscosity terms [7].

The point-to-point first and second channels of the pressure terms are the same, which is theoretically proven in Appendix C. For the statistical characteristics of the pressure term of helicity transfer in compressible turbulent flows, we performed a detailed analysis in our previous paper [7]. Regarding the viscosity terms, their reduced forms are the same in incompressible turbulent flows but are different in compressible turbulent flows. The specific derivation is also given in Appendix C.

By comparing the governing equations of filtered helicity \bar{H} and Favre-filtered helicity \tilde{H} , we can conclude that only Favre-filtered helicity \tilde{H} is appropriate for investigating the helicity cascade in compressible turbulent flows. Owing to the presence of a large-scale hydrodynamic source term, unresolved presence, and viscous terms in Eq. (A5), the intrinsic mechanism of the transfer of filtered helicity \bar{H} is unclear. In other words, too many unresolved terms need to be modeled in this form of large-scale helicity.

IV. DUAL CHANNELS OF HELICITY TRANSFER

A. SGS terms

From Eqs. (17) and (18), large discrepancies in the helicity cascade exist between incompressible and compressible turbulent flows. In this section we investigate the statistical characteristics of the first and second channels of the helicity cascade on the basis of the above numerical results, especially under the influence of compressibility.

In our previous work [56], we theoretically proved the equality relation of the ensemble averages of the first and second channels in three-dimensional turbulent flows. The equality relation applies to the dual channels of the helicity cascade in compressible turbulent flows, and we also employ the following identical relation:

$$\nabla \cdot (\mathbf{a} \times \mathbf{b}) = \mathbf{b} \cdot (\nabla \times \mathbf{a}) - \mathbf{a} \cdot (\nabla \times \mathbf{b}), \quad (25)$$

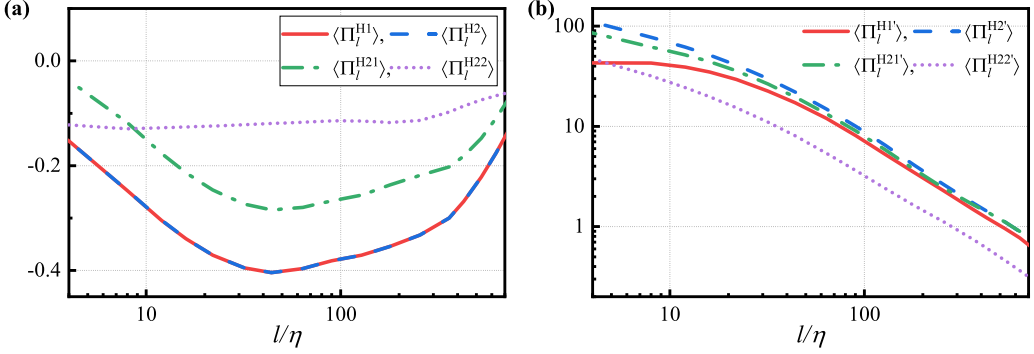


FIG. 3. The ensemble averages (a) and rms (b) of the first and second channels of the helicity cascade.

with $\mathbf{a} = \tilde{\mathbf{u}}$ and $\mathbf{b} = \nabla \cdot (\tilde{\rho} \tilde{\boldsymbol{\tau}}) / \tilde{\rho}$ for any filter width. The expressions of the first- and second-channel helicity fluxes can be rewritten as

$$\Pi_l^{H1} = -\tilde{\rho} \tilde{\tau}_{ij} \frac{\partial}{\partial x_j} \left(\frac{\tilde{\omega}_i}{\tilde{\rho}} \right) \equiv -\frac{\partial}{\partial x_j} (\tilde{\tau}_{ij} \tilde{\omega}_i) + \frac{\tilde{\omega}_i}{\tilde{\rho}} \frac{\partial}{\partial x_j} (\tilde{\rho} \tilde{\tau}_{ij}), \quad (26)$$

$$\begin{aligned} \Pi_l^{H2} &= -\epsilon_{ikl} \frac{\partial \tilde{\rho} \tilde{\tau}_{lj}}{\partial x_k} \frac{\partial}{\partial x_j} \left(\frac{\tilde{u}_i}{\tilde{\rho}} \right) - \tilde{\rho} \tilde{\tau}_{ij} \frac{\partial}{\partial x_j} \left[\epsilon_{ikl} \tilde{u}_k \frac{\partial}{\partial x_l} \left(\frac{1}{\tilde{\rho}} \right) \right] \\ &\equiv -\frac{\partial}{\partial x_j} \left[\epsilon_{ikl} \frac{\partial \tilde{\rho} \tilde{\tau}_{lj}}{\partial x_k} \frac{\tilde{u}_i}{\tilde{\rho}} + \tilde{\rho} \tilde{\tau}_{ij} \epsilon_{ikl} \tilde{u}_k \frac{\partial}{\partial x_l} \left(\frac{1}{\tilde{\rho}} \right) \right] + \tilde{u}_i \epsilon_{ijk} \frac{\partial}{\partial x_k} \left(\frac{\partial \tilde{\rho} \tilde{\tau}_{lj}}{\partial x_l} \frac{1}{\tilde{\rho}} \right). \end{aligned} \quad (27)$$

Hence, the difference of the first- and second-channel helicity flux can be expressed as

$$\begin{aligned} \Delta &= \Pi_l^{H1} - \Pi_l^{H2} \equiv \frac{\tilde{\omega}_i}{\tilde{\rho}} \frac{\partial}{\partial x_j} (\tilde{\rho} \tilde{\tau}_{ij}) - \tilde{u}_i \epsilon_{ijk} \frac{\partial}{\partial x_k} \frac{\partial \tilde{\rho} \tilde{\tau}_{lj}}{\partial x_l} \frac{1}{\tilde{\rho}} \\ &\quad + \frac{\partial}{\partial x_j} \left[\epsilon_{ikl} \frac{\partial \tilde{\rho} \tilde{\tau}_{lj}}{\partial x_k} \frac{\tilde{u}_i}{\tilde{\rho}} + \tilde{\rho} \tilde{\tau}_{ij} \epsilon_{ikl} \tilde{u}_k \frac{\partial}{\partial x_l} \left(\frac{1}{\tilde{\rho}} \right) - \tilde{\tau}_{ij} \tilde{\omega}_i \right] \\ &\equiv \frac{\partial}{\partial x_j} \left[\epsilon_{jkl} \tilde{u}_k \frac{\partial \tilde{\rho} \tilde{\tau}_{lj}}{\partial x_j} \frac{1}{\tilde{\rho}} + \epsilon_{ikl} \frac{\partial \tilde{\rho} \tilde{\tau}_{lj}}{\partial x_k} \frac{\tilde{u}_i}{\tilde{\rho}} + \tilde{\rho} \tilde{\tau}_{ij} \epsilon_{ikl} \tilde{u}_k \frac{\partial}{\partial x_l} \left(\frac{1}{\tilde{\rho}} \right) - \tilde{\tau}_{ij} \tilde{\omega}_i \right]. \end{aligned} \quad (28)$$

Making an ensemble average on the above expression, it can be simplified according to the three-dimensional homogeneity,

$$\langle \Delta \rangle = \langle \Pi_l^{H1} \rangle - \langle \Pi_l^{H2} \rangle \equiv 0. \quad (29)$$

Hence, the ensemble averages of the first- and second-channel helicity fluxes are equal, and the equality relation is numerically confirmed in Fig. 3(a).

In Fig. 3(a) we also present the ensemble averages of the first and second terms of the second channel of the helicity cascade. The first term is dominant except at relatively small scales. The second term is associated with the density gradient, and the positive and negative cancellations in the compression and expansion regions lead to smaller amplitudes. With decreasing length scale, the scale accumulation effect does not increase, and the second term of the second channel is nearly constant at small scales. This regulation is similar to the scale effect of pressure terms present in the governing equations of large-scale kinetic energy and helicity [7,69,70]. In addition, we show their root-mean-square (rms) values in Fig. 3(b). The fluctuations of the second channel are larger than those of the first channel, and the fluctuations of the first term are also larger than those of the second term. With decreasing length scale, the fluctuations begin to increase gradually, which reveals greater fluctuations at small scales. For the second channel, the fluctuations mainly originate from the first term.

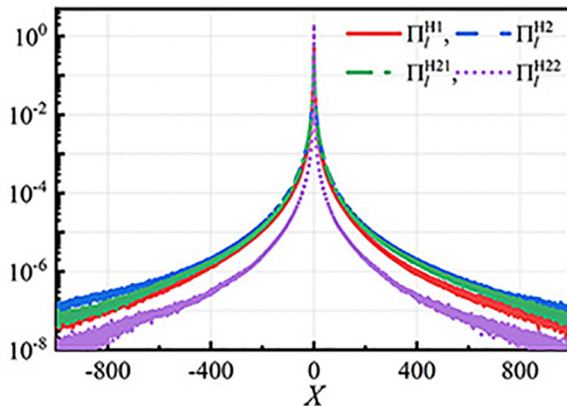


FIG. 4. PDF of the first and second channels of the helicity cascade and the first and second terms of the second channel with filter width $l/\eta = 32$.

We show the PDF of the first and second channels of the helicity cascade and the first and second terms of the second channel in Fig. 4 with a typical filter width $l/\eta = 32$. The corresponding PDFs are consistent with the conclusions in Fig. 3(b). Extreme events [71], which fluctuate more strongly by two orders than the mean of the second term of the second channel, are currently less common, whereas extreme events of the first term of the second channel are more common, for both the left and right tails. Their discrepancies are similar, the orders for high-order moments ($n \geq 2$, where n is the order) of the second channel are larger than those of the first channel, and the second term is smaller than the first term of the second channel. In other words, the skewness of the second channel is larger than that of the first channel, and the skewness of the second term of the second channel is smaller than that of the first term of the second channel. This regulation also applies to their discrepancies in flatness.

Similar to the refined similarity hypothesis of a local energy flux proposed by Kraichnan [72] and a local helicity flux proposed by Chen *et al.* [39], we can define a set of scaling exponents $\zeta(p)$ for a helicity cascade at length scale l as

$$\langle |l^2 \Pi_l^X|^{p/3} \rangle \sim l^{\zeta(p)}, \quad (30)$$

where X denotes H1 for the first channel, H2 for the second channel, H21 for the first term of the second channel, and H22 for the second term of the second channel. In Fig. 5 we show the structure functions of the first and second channels and the first and second terms of the second channel at different length scales for order p from 1 to 8. For all the results in log-log coordinates, the curves within the x axis from $l = 60\eta$ to $l = 400\eta$ exhibit a nearly linear property, and we fit all the curves within this region to obtain the slopes using the extended self-similarity procedure [73].

The above-fitted slopes are shown in Fig. 6, and the classic $p/3$ scaling exponent marked as K41 is also plotted to compare the intermittency discrepancies. The scaling exponent of the second channel deviates more from K41 without considering any intermittency, in contrast to the first channel. This means that the second channel is more intermittent than the first channel is, and the regulation is consistent with our previous conclusion regarding incompressible turbulent flows [56]. For the intermittency discrepancies of the first and second terms of the second channel, the results in Fig. 6(b) reveal that the first term is more intermittent, and this conclusion is also consistent with the PDF discrepancy in Fig. 4.

In contrast to the first channel, the scaling exponent of the second channel tends to saturate with order $p \geq 6$, and both the first and second terms of the second channel also tend to saturate with order $p \geq 6$. In incompressible turbulent flows, whichever channel we choose, the scaling exponents of the helicity cascade increase monotonically [39,56]. Previous studies confirmed that the structure

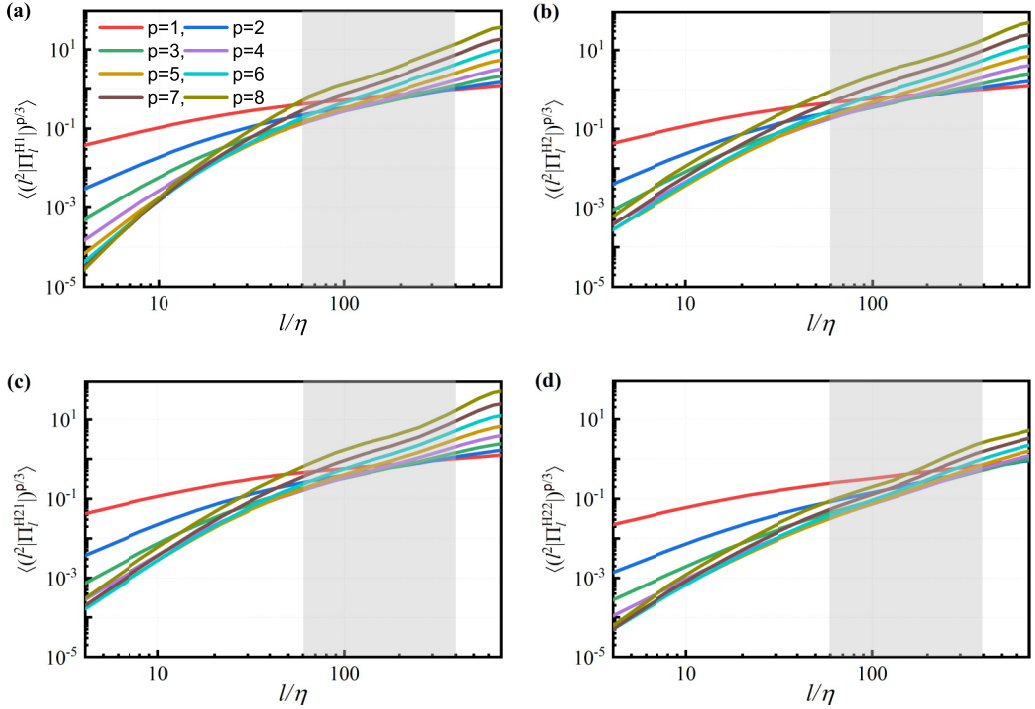


FIG. 5. Structure functions of the first channel (a), the second channel (b), the first term of the second channel (c), and the second term of the second channel (d).

functions saturate due to the appearance of shocklets in compressible turbulent flows [74–76] and that compressibility plays an important role in intermittent turbulence. As we stated previously, the second channel is more closely associated with variable density or compressibility, and the saturated scaling exponents of the second channel confirm this theoretical analysis.

To evaluate the compression or expansion effects on the first and second channels of the helicity cascade, we present the ensemble averages of the first and second channels conditioned in the compression regions ($\theta_l < 0$) and expansion regions ($\theta_l > 0$) in Fig. 7(a). In contrast to those in the expansion regions, the flows in the compression regions dominate the helicity cascade for

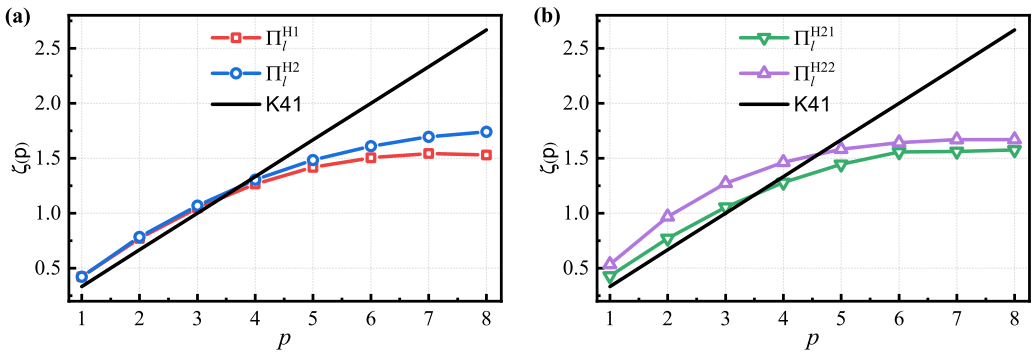


FIG. 6. Scaling exponents of the first and second channels (a) and the first and second terms of the second channel (b). The black solid line refers to the K41 theory [77].

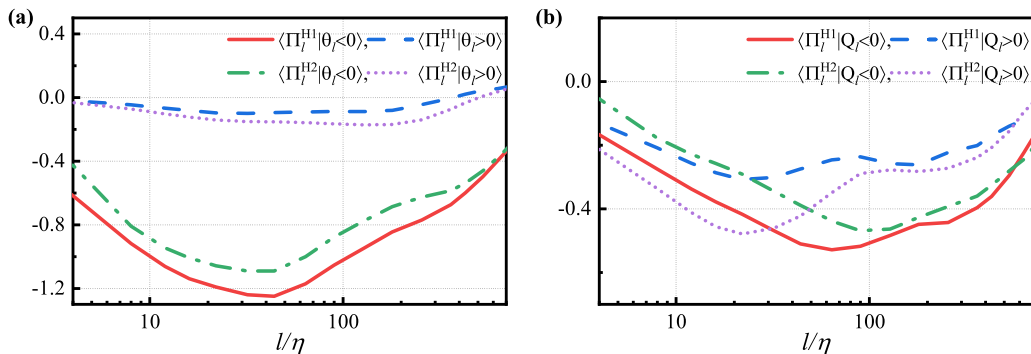


FIG. 7. (a) The ensemble averages of the first and second channels in compression regions ($\theta_l < 0$) and expansion regions ($\theta_l > 0$). (b) The ensemble averages of the first and second channels in the strain regions ($Q_l < 0$) and rotation regions ($Q_l > 0$).

both the first and second channels. However, the equality relation is broken in the compression or expansion region because the three-dimensional homogeneity cannot be satisfied in only the compression or expansion region. If the sample points are large enough, the statistical discrepancies in the compression and expansion regions would be negligible. In compression regions, the first channel has a dominant role with larger amplitudes. Nevertheless, the second channel dominates the helicity cascade in expansion regions. The different roles of the first and second channels reveal the complexity of the interscale transfer of helicity in compressible turbulent flows.

In Fig. 7(b) we show the ensemble averages of the first and second channels in the strain regions ($Q_l < 0$) and rotation regions ($Q_l > 0$), and Q_l is the second invariant of the velocity gradient at scale l [78–80]. Overall, the discrepancies in the strain and rotation effects are similar to those in the compression and expansion effects. This means that the first channel is dominant in the strain regions, and the second channel is dominant in the rotation regions. However, for the first or second channel, only the flows at large scales in the strain regions are dominant, and the flows at small scales in the rotation regions are dominant. The critical length scales that differ in terms of the roles of the strain and rotation regions are approximately 30η , which also distinguishes the inertial and dissipation regions. The dominant strain regions at relatively large scales for the helicity cascade are consistent with the energy cascade process, which is also concentrated within large strain regions [81]. At relatively small scales, the rotation motion begins to affect the helicity transfer across scales. Although the ensemble averages of cross-scale transfer at small scales are small, the local fluctuations are still very strong [82]. Hence, it is also worth exploring their statistical characteristics at small scales.

The compression or expansion effects on the first and second channels are shown in Fig. 8. To the naked eye, the compression regions are dominant, and even some small expansion regions are present. The velocity divergence is related to shocklets in the present numerical simulations. The compression regions tend to include large-scale sheet structures, which also confirms that shocklets play an important role in helicity transfer.

The compression and expansion effects on the first and second terms of the second channel are numerically explored in Fig. 9(a), and flows in the compression regions dominate the first and second terms of the second channel. In compression regions, the first term is dominant at large scales, whereas the second term is dominant at small scales. The sign of the second term in the expansion regions is positive, and it corresponds to an inverse helicity cascade. As we stated previously, the second term is present only in compressible flows without more species. Hence, we can conclude that the expansion motions could promote the inverse helicity cascade via the second term of the second channel.

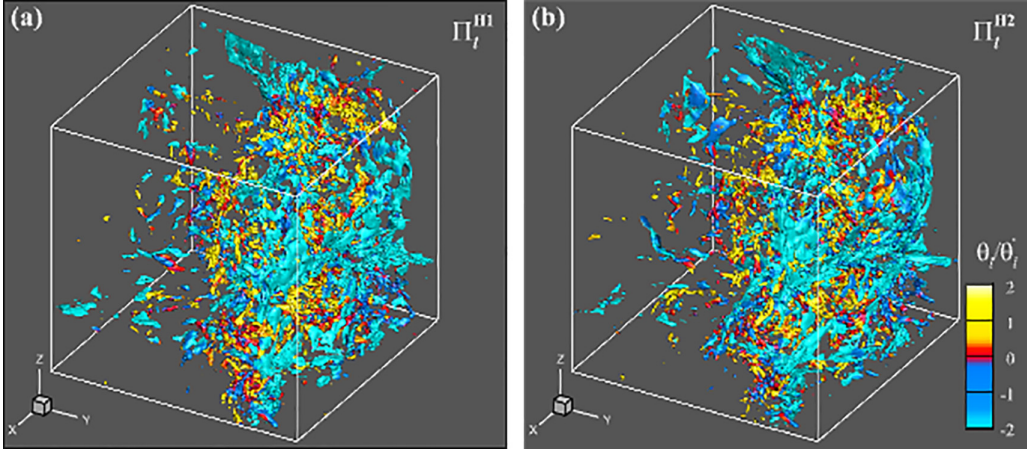


FIG. 8. Three-dimensional isosurfaces of the first channel (a) and second channel (b) rendered by local velocity divergence with filter width $l = 32\eta$.

For the strain and rotation effects on the first and second terms of the second channel, we present their ensemble averages conditioned in the strain and rotation regions in Fig. 9(b). At large scales, the strain regions dominate the first and second terms. However, at small scales, the rotation regions dominate the first and second terms. In the strain or rotation regions, the first term is dominant at large scales, and the second term is dominant at small scales. The critical scales lie within the dissipation regions.

The compression or expansion effects on the second term of the second channel are further numerically investigated with different filter widths in Fig. 10 via the conditional averaging method [58,83]. In expansion regions, the ensemble averages of the second term of the second channel are positive. In addition, their amplitudes increase with increasing expansion degree. Its ensemble average is nearly zero around zero velocity divergence, which indicates that the second term of the second channel depends on compression or expansion in the present numerical simulations. In compression regions, their amplitudes also increase with increasing compressibility.

In Fig. 11 we show the three-dimensional isosurfaces of the first and second terms rendered by local velocity divergence. Both spatial distributions confirm the dominant roles of the compression

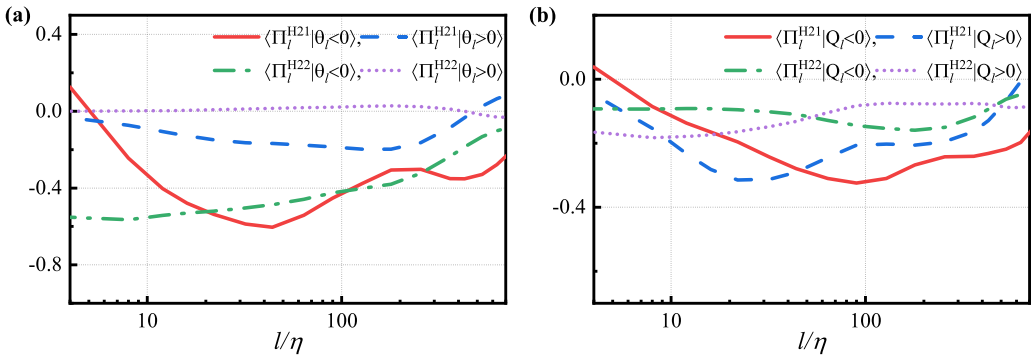


FIG. 9. (a) The ensemble averages of the first and second terms of the second channel of the helicity cascade in the compression regions ($\theta_l < 0$) and expansion regions ($\theta_l > 0$). (b) The ensemble averages of the first and second terms of the second channel of the helicity cascade in the strain regions ($Q_l < 0$) and rotation regions ($Q_l > 0$).

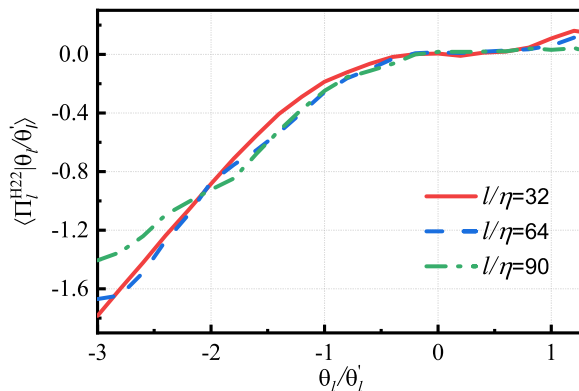


FIG. 10. The ensemble averages of the second term of the second channel of the helicity cascade are conditioned on the local velocity divergence with filter widths $l/\eta = 32$, $l/\eta = 64$, and $l/\eta = 90$.

regions. Nevertheless, the dominating degree of the first term of the compression regions is smaller than that of the second term. The overwhelming role of the compression regions of the second term confirms that the second term of the second channel is associated with compressibility.

B. Viscosity term

The role of viscosity in the evolution of helicity is completely different from that in the evolution of kinetic energy. From the perspective of governing equations, viscosity plays a statistically dissipative role in the transfer of kinetic energy into internal energy. Nevertheless, viscosity creates a bridge for helicity transfer between different chirality. Specifically, if viscosity plays a dissipation role for left-chirality helicity, it must play a generating role for right-chirality helicity, and vice versa. Hence, the kinetic energy-governing equation must be accompanied by an internal energy governing equation to describe the energy path correctly. However, the helicity-governing equation does not need to couple with other equations. In addition, viscosity also has other effects [5], such as mediating the process of reconnecting vortex lines, causing vorticity to diffuse away from the vortex centerline [84–87].

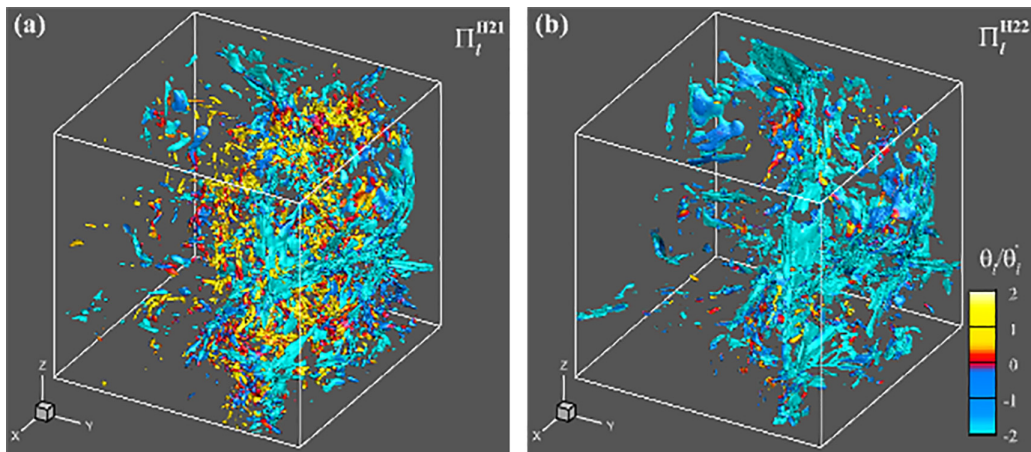


FIG. 11. Three-dimensional isosurfaces of the first term (a) and second term (b) of the second channel of the helicity cascade rendered by local velocity divergence with filter width $l = 32\eta$.

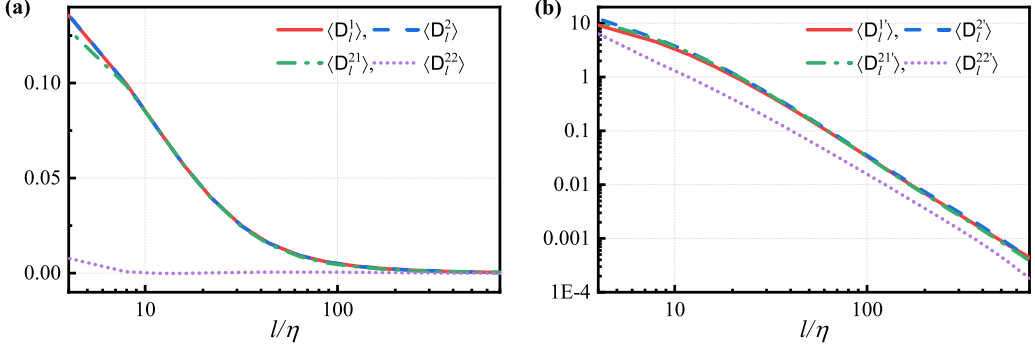


FIG. 12. The ensemble averages (a) and rms (b) of the first and second channels of the viscosity terms and the first and second terms of the second channel.

According to the previous derivation, there are also two channels of viscosity terms for helicity-governing equations in compressible turbulent flows, especially compared with incompressible turbulent flows. The second channel can be further decomposed into two terms, which also originate from the variable density effect. The filtered viscosity terms should satisfy the inviscid criteria proposed by Aluie [63] and Zhao and Aluie [88], which indicates that the viscosity effect should not be negligible only at small scales. The numerical results of the viscosity terms shown in Fig. 12(a) are consistent with the inviscid criteria, which proves that the filter operation in the present numerical analysis is valid. In Fig. 12 we present the ensemble averages and rms of the first and second channels of the viscosity terms and the first and second terms of the second channel. The identical relation of Eq. (25) also applies to the relation of the first and second channels of the viscosity terms, with $\mathbf{a} = \tilde{\mathbf{u}}$ and $\mathbf{b} = \nabla \sigma / \bar{\rho} / \text{Re}$. This means that the ensemble averages of the first and second channels of the viscosity terms are equal, and the numerical results in Fig. 12(a) confirm the identical relation. The first term of the second-channel viscosity term is similar to its form in incompressible turbulent flows, and the second term originates from the baroclinic effect of the velocity and density gradient. The numerical results in Fig. 12(a) reveal that the first term of the second-channel viscosity term is dominant, in contrast to the second term. The degrees of fluctuation are shown in Fig. 12(b). The rms of the second-channel viscosity term is larger than that of the first channel, and the rms of the first term of the second-channel viscosity term is larger than that of the second term. These regulations are consistent with those of SGS terms.

The corresponding PDF is shown in Fig. 13. The PDF of the first-channel viscosity term is larger than that of the second-channel viscosity term at the left and right tails, and it means that the second-channel viscosity term is more intermittent than the first-channel viscosity term. The PDF of the first term of the second-channel viscosity term is larger than that of the second term, and it means that the first term of the second-channel viscosity term is more intermittent than the second term. To conclude, the second term of the second-channel viscosity term seems to be statistically negligible. However, some discrepancies may exist in the compression or expansion regions because its definition determines that it is associated with the density gradient.

To investigate the compressibility effects on the above viscosity terms, we present their ensemble averages in the compression and expansion regions in Fig. 14. The ensemble averages of the first- and second-channel viscosity terms in the compression regions are larger than those in the expansion regions, which means that the compression effect is dominant for viscosity dissipation. For the first term of the second-channel viscosity term, the compression effect is also dominant. However, the second term of the second-channel viscosity term depends on the compression and expansion motions. In compression regions, the ensemble averages of the second term are positive, which plays a dissipation role in the helicity transfer. In expansion regions, the ensemble averages of the second term are negative, which plays a generation role in the helicity transfer. This conclusion is

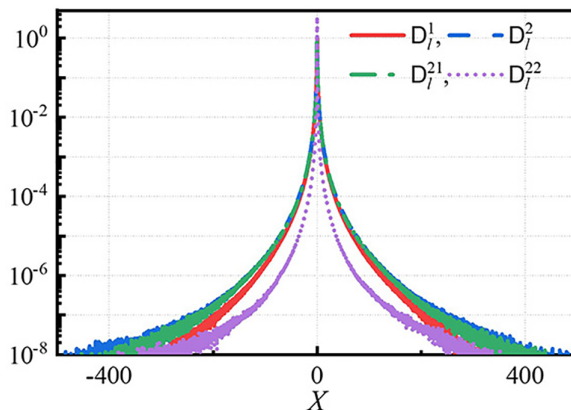


FIG. 13. PDF of the first and second channels of the viscosity terms and the first and second terms of the second channel with filter width $l/\eta = 8$.

further validated in Fig. 15, which shows the ensemble average of the second term of the second-channel viscosity term conditioned on local velocity divergence with different filter widths. The larger ensemble averages at small scales originate from small-scale shear. With increasing expansion motion, the amplitudes of the second term also increase. This correlation is consistent with the corresponding regulation of the expansion effect on the second term of the second-channel helicity flux shown in Fig. 10.

It can be concluded that an expansion motion can promote inverse helicity transfer through the second term of the second-channel viscosity term, which leads to high helicity distributions. This regulation is consistent with our previous work [55], which revealed that expansion motion can promote inverse helicity transfer through nonlinear terms in addition to SGS terms and viscosity terms.

Helicity evolution is associated with vortex structures. The rotation motion is dominant within the vortex structures, and the strain motion is dominant between vortex pairs [81]. The ensemble averages of the above viscosity terms in the strain and rotation regions are shown in Fig. 16. Discrepancies in the first- and second-channel viscosity terms exist in the strain and rotation regions. For the first channel, strain motion dominates the viscosity dissipation process, which is similar to the viscosity dissipation of kinetic energy [71,89]. Nevertheless, the rotation motion dominates the

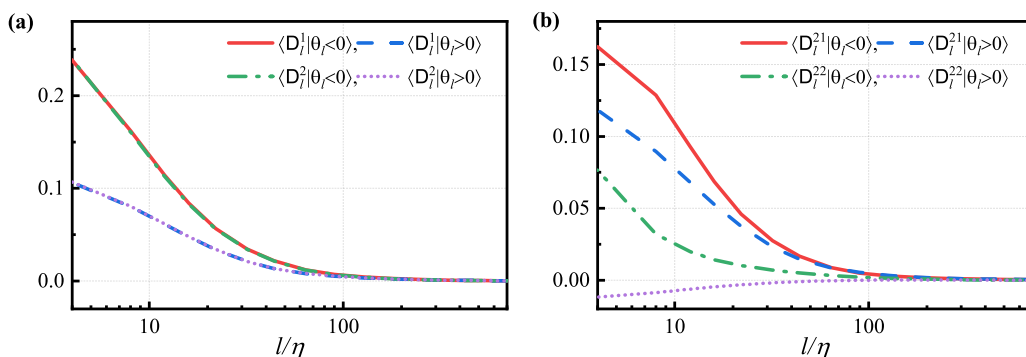


FIG. 14. (a) The ensemble averages of the first and second channels of the viscosity terms in the compression and expansion regions. (b) The ensemble averages of the first and second terms of the second-channel viscosity term in the compression and expansion regions.

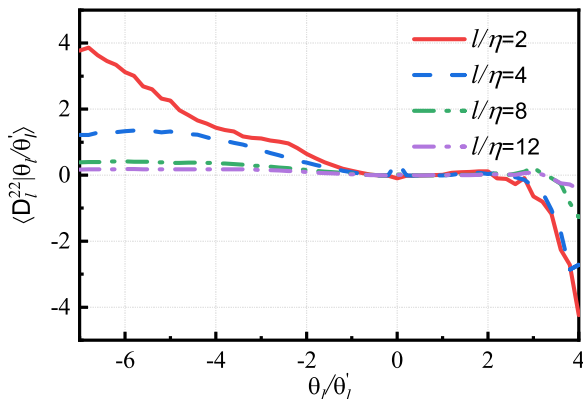


FIG. 15. The ensemble averages of the second term of the second channel of viscosity terms conditioned on local velocity divergence with filter widths $l/\eta = 2$, $l/\eta = 4$, $l/\eta = 8$, and $l/\eta = 12$.

viscosity dissipation process for the second channel. This means that viscosity dissipation occurs both inside and outside of vortex structures, with the first channel dominating the outside and the second channel dominating the inside of vortex structures. With decreasing length scale, the dominant role of the second channel in the rotation regions becomes more apparent. We infer that below the Kolmogorov scale in the dissipation ranges, the rotation motion of the fluid element seems to be similar to rigid rotation [90,91], and the second-channel viscosity term is important. The dominant role of the second channel in the rotation regions is further reflected in the first term of the second-channel viscosity term in Fig. 16(b).

V. CONCLUSIONS AND DISCUSSION

In this work, we explore the large-scale helicity transfer in compressible helical turbulent flows and confirm the existence of the dual-channel characteristics of SGS and viscosity terms extended from our previous dual-channel theory of helicity cascades in incompressible turbulent flows [56]. We can prove theoretically that dual channels exist only in SGS terms for large-scale helicity transfer in incompressible turbulent flows, and dual channels exist only in SGS and viscosity terms in compressible turbulent flows. The dual-channel SGS and viscosity terms exhibit different statistical characteristics, especially under the effects of compression, expansion, strain, and rotation motions.

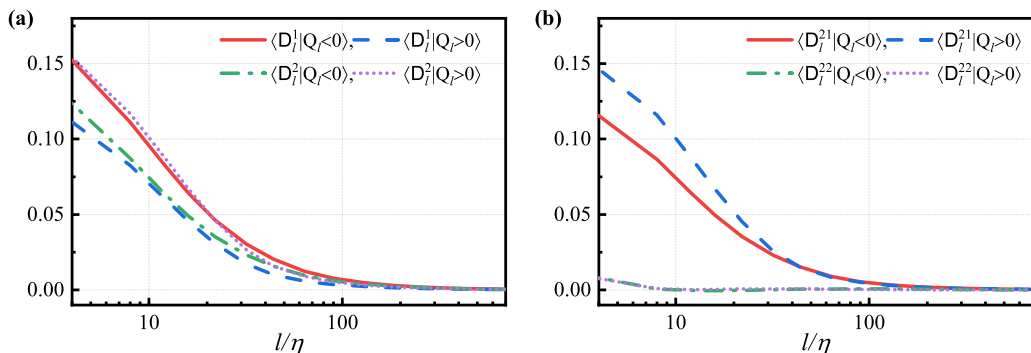


FIG. 16. (a) The ensemble averages of the first and second channels of the viscosity terms in the strain and rotation regions. (b) The ensemble averages of the first and second terms of the second-channel viscosity term in the strain and rotation regions.

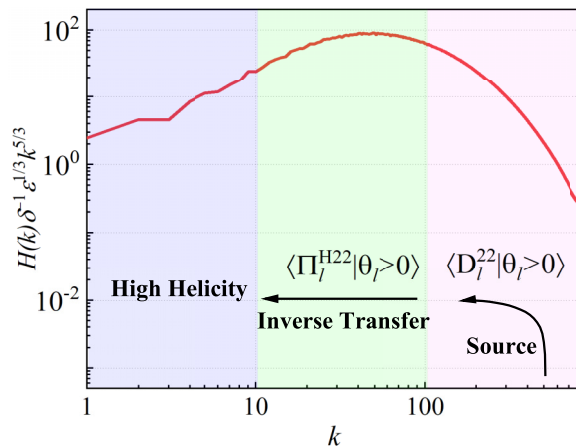


FIG. 17. Normalized helicity spectrum.

A suitable definition for large-scale helicity in compressible turbulent flows is selected to represent the conservative character of a helicity transfer, eliminating the pressure and viscosity terms. Like inviscid criteria for large-scale kinetic energy in compressible turbulent flows [63,88], large-scale helicity should involve the Favre-filtered velocity and vorticity, which is defined as $\tilde{H} = \tilde{\mathbf{u}} \cdot \tilde{\boldsymbol{\omega}}$. Equation (15) indicates that only SGS transfer occurs in the inertial subrange; it does not consider the pressure and viscosity terms.

On the basis of a simple algebraic operation, we can prove that the two point-to-point pressure terms originating from the momentum and vorticity governing equations are the same in compressible turbulent flows, and the dual-channel characteristics of the SGS and viscosity terms are highlighted. According to the three-dimensional homogeneity condition, the ensemble averages of the first and second channels of the SGS and viscosity terms are equal, but the second channels are more intermittent. The higher intermittency results from the density gradient, which is associated with shocklets. Similar to the kinetic energy cascade, the compression motions dominate the dual channel of the helicity cascade. The strain and rotation motions also have an important effect on the dual channel of the helicity cascade. The first channel is dominant in the strain regions, and the second channel is dominant in the rotation regions. Hence, the dissipation mechanism of large-scale helicity is different from that of large-scale kinetic energy. For kinetic energy, viscous dissipation mainly occurs in the strain regions, which correspond to the intersections of two corotating vortices. Nevertheless, viscous dissipation of helicity occurs both inside and outside of vortex structures through the first and second channels, respectively. At smaller scales within dissipation ranges, the rotation motions are dominant for both the first and second channels of SGS helicity transfer. This can be explained by the fact that the rotation motions become apparent as the length scales decrease.

The second-channel SGS and viscosity terms can be further decomposed into two terms. The first terms are dominant, and their intermittencies are higher than those of the second term. The compression motions are also dominant for the first and second terms of the second-channel SGS and viscosity terms. In expansion regions, the ensemble averages of the second term of the second-channel SGS and viscosity terms are positive and negative, respectively. Both terms correspond to an inverse helicity transfer. Combined with the expansion effect on the chirality-transfer process [55], we can conclude that the expansion motions promote inverse helicity transfer, which is reflected in the second channels of the SGS and viscosity terms. In addition, we schematically summarize the proposed induced mechanism in Fig. 17. In fully developed helical turbulent flows, the helicity spectrum obeys the power-law solution $H(k) \sim C_H \delta \varepsilon^{-1/3} k^{-5/3}$, where C_H is the Kolmogorov constant of the helicity spectrum [25,39]. In Fig. 17 we show the normalized helicity spectrum in the present numerical simulations with a high Reynolds number. Owing to the limitation of the

computational cost, the present Reynolds number is still not large enough to exhibit an apparent inertial subrange. At small scales, the second term of the second-channel viscosity in expansion regions ($D_l^{22}|\theta_l > 0$) serves as a source of helicity generation. At medium scales, the second term of the second-channel helicity flux in expansion regions ($\Pi_l^{H22}|\theta_l > 0$) serves as an inverse cross-scale transfer mechanism. It transfers the helicity generated or deposited at small scales to large scales, and large-scale helical structures can be sustained to some extent.

In summary, we comprehensively study large-scale helicity transfer in compressible turbulent flows and highlight the dual-channel characteristics of the SGS and viscosity terms. From the perspective of the vortex dynamics, the dual channels of the helicity transfer involve the vortex twisting and stretching processes, under the influence of the compressibility. Meanwhile, it also uncovers the inverse helicity transfer process. The inverse helicity transfer mechanism can be uncovered through dual-channel helicity transfer in expansion regions, and it is premised on investigating the effects of helicity on turbulence statistics. The rotation motions are also regarded as important dissipation mechanisms through the second-channel viscosity term, in contrast to previously described strain motions.

ACKNOWLEDGMENTS

This work is funded by the National Natural Science Foundation of China (Grants No. 12302281, No. 11975053, No. 12232018, and No. 91852203). Z. Y. is also supported by the China Postdoctoral Science Foundation (No. 2022M710459). All the numerical simulations were performed on supercomputers in China. In addition, we would like to express our honest appreciation to Dr. F. Tong for many useful discussions.

APPENDIX A: GOVERNING EQUATION OF THE LARGE-SCALE HELICITY $\bar{H} = \bar{u} \cdot \bar{\omega}$ IN COMPRESSIBLE TURBULENT FLOWS

Expanding Eq. (3b) without considering external force and subtracting Eq. (3a), we can obtain the following velocity governing equation:

$$\frac{\partial u_i}{\partial t} + u_j \frac{\partial u_i}{\partial x_j} = -\frac{1}{\rho} \frac{\partial p}{\partial x_i} + \frac{1}{\text{Re}} \frac{1}{\rho} \frac{\partial \sigma_{ij}}{\partial x_j}. \quad (\text{A1})$$

Performing a curl operation on Eq. (A1), we can obtain the following governing equation of vorticity in compressible flows:

$$\frac{\partial \omega_i}{\partial t} + u_j \frac{\partial \omega_i}{\partial x_j} = \omega_j \frac{\partial u_i}{\partial x_j} - \omega_i \theta - \epsilon_{ijk} \frac{\partial}{\partial x_j} \left(\frac{1}{\rho} \frac{\partial p}{\partial x_k} \right) + \frac{1}{\text{Re}} \epsilon_{ijk} \frac{\partial}{\partial x_j} \left(\frac{1}{\rho} \frac{\partial \sigma_{kl}}{\partial x_l} \right), \quad (\text{A2})$$

where ϵ_{ijk} is the Levi-Chivita tensor.

Next, filter operations are performed on Eqs. (A1) and (A2), and the following governing equations of filtered velocity and vorticity can be obtained:

$$\frac{\partial \bar{u}_i}{\partial t} + \bar{u}_j \frac{\partial \bar{u}_i}{\partial x_j} + \bar{u}_i \bar{\theta} = -\frac{\partial \bar{\tau}_{ij}}{\partial x_j} - \bar{u}_i \bar{\theta} - \frac{1}{\rho} \frac{\partial \bar{p}}{\partial x_i} + \frac{1}{\text{Re}} \frac{1}{\rho} \frac{\partial \bar{\sigma}_{ij}}{\partial x_j}, \quad (\text{A3})$$

$$\frac{\partial \bar{\omega}_i}{\partial t} + \bar{u}_j \frac{\partial \bar{\omega}_i}{\partial x_j} + \bar{\omega}_i \bar{\theta} = \bar{\omega}_j \frac{\partial \bar{u}_i}{\partial x_j} - \frac{\partial \bar{\gamma}_{ij}}{\partial x_j} - \epsilon_{ijk} \frac{\partial}{\partial x_j} \left(\frac{1}{\rho} \frac{\partial \bar{p}}{\partial x_k} \right) + \frac{1}{\text{Re}} \epsilon_{ijk} \frac{\partial}{\partial x_j} \left(\frac{1}{\rho} \frac{\partial \bar{\sigma}_{kl}}{\partial x_l} \right), \quad (\text{A4})$$

where $\bar{\tau}_{ij}$ is the subgrid-scale stress defined as $\bar{\tau}_{ij} = \overline{u_i u_j} - \bar{u}_i \bar{u}_j$ and where $\bar{\gamma}_{ij}$ is the subgrid-scale vortex stretching stress defined as $\bar{\gamma}_{ij} = \overline{u_j \omega_i} - \bar{u}_j \bar{\omega}_i - (\bar{u}_j \bar{\omega}_i - \bar{u}_i \bar{\omega}_j)$.

According to the definition of \bar{H} , we can obtain the governing equation of large-scale helicity \bar{H} by combining Eqs. (A3) and (A4) as follows:

$$\frac{\partial \bar{H}}{\partial t} + \frac{\partial \bar{J}_j}{\partial x_j} = -\bar{H} \bar{\theta} - \Pi_l^{\bar{H}1} - \Pi_l^{\bar{H}2} + \overline{u_i \theta \omega_i} + \bar{\Phi} + \bar{D}, \quad (\text{A5})$$

where \bar{J}_j is the spatial transport term, which is defined as follows:

$$\bar{J}_j = \bar{u}_j \bar{H} - (1/2) \bar{u}_i \bar{u}_i \bar{\omega}_j + \bar{\omega}_i \bar{\tau}_{ij} + \bar{u}_i \bar{\gamma}_{ij}. \quad (\text{A6})$$

Here, $\Pi_l^{\bar{H}1}$ and $\Pi_l^{\bar{H}2}$ refer to the first and second channels of the helicity cascade similar to those in the incompressible case, respectively, and are defined as follows:

$$\Pi_l^{\bar{H}1} = \bar{\tau}_{ij} \frac{\partial \bar{\omega}_i}{\partial x_j}, \quad \Pi_l^{\bar{H}2} = \bar{\gamma}_{ij} \frac{\partial \bar{u}_i}{\partial x_j}. \quad (\text{A7})$$

$\bar{\Phi}$ refers to the pressure term, which is defined as follows:

$$\bar{\Phi} = -\frac{1}{\rho} \frac{\partial \bar{p}}{\partial x_i} \bar{\omega}_i + \frac{\epsilon_{ijk}}{\rho^2} \frac{\partial \rho}{\partial x_j} \frac{\partial \bar{p}}{\partial x_k} \bar{u}_i. \quad (\text{A8})$$

\bar{D} denotes the viscous term, which is defined as follows:

$$\bar{D} = \frac{1}{\text{Re}} \frac{1}{\rho} \frac{\partial \bar{\sigma}_{ij}}{\partial x_j} \bar{\omega}_i + \frac{1}{\text{Re}} \epsilon_{ijk} \frac{\partial}{\partial x_j} \left(\frac{1}{\rho} \frac{\partial \bar{\sigma}_{kl}}{\partial x_l} \right) \bar{u}_i. \quad (\text{A9})$$

The first term on the r.h.s. of Eq. (A5) only includes a large-scale flow field, and it acts as a resource term at all scales, similar to the vortex stretching term of the enstrophy governing equation in three-dimensional turbulent flows. The presence of large-scale source terms originating from the velocity field breaks the conservative characteristic of the helicity cascade, except for the pressure and viscosity terms in compressible turbulent flows. The other terms on the r.h.s. of Eq. (A5) involve large- and small-scale flow fields. In particular, the two expressions of the interscale helicity are the same as those in incompressible turbulent flows.

APPENDIX B: TENSOR GEOMETRY OF THE FIRST TERM OF THE SECOND-CHANNEL HELICITY CASCADE

For the convenience of tensor analysis, we introduce a density-weighted velocity \mathbf{v} and a filtered density-weighted velocity \mathbf{w} as follows:

$$\mathbf{v} = \sqrt{\rho} \mathbf{u}, \quad \mathbf{w} = \sqrt{\rho} \tilde{\mathbf{u}}. \quad (\text{B1})$$

This weighted velocity form is suitable for investigating the spectral properties of physical variables in compressible flows, such as kinetic energy [92]. The SGS stress can be rewritten as follows:

$$\bar{\rho} \bar{\tau}_{ij} \equiv \overline{\sqrt{\rho} u_i \cdot \sqrt{\rho} u_j} - \sqrt{\rho} \tilde{u}_i \cdot \sqrt{\rho} \tilde{u}_j \equiv \bar{v}_i \bar{v}_j - w_i w_j. \quad (\text{B2})$$

Using the above definitions, the tensor operation of the first term of the SGS stress involved in the first term can be written as follows:

$$\begin{aligned} \epsilon_{ijk} \frac{\partial}{\partial x_j} \left[\frac{\partial}{\partial x_m} (\overline{v_k v_m}) \right] &= \epsilon_{ijk} \frac{\partial}{\partial x_j} \left(\overline{v_m \frac{\partial v_k}{\partial x_m}} + v_k \frac{\partial \overline{v_m}}{\partial x_k} \right) \\ &= \epsilon_{ijk} \frac{\partial}{\partial x_j} \left[\overline{\epsilon_{kmn} \omega_m v_n} + \frac{\partial}{\partial x_k} \left(\frac{1}{2} \overline{v_m v_m} \right) + v_k \frac{\partial \overline{v_m}}{\partial x_m} \right] \\ &= v_j \frac{\partial \bar{\omega}_i}{\partial x_j} - \bar{\omega}_j \frac{\partial \bar{u}_i}{\partial x_j} + 2 \bar{\omega}_i \bar{\theta} + \epsilon_{ijk} \frac{\partial \bar{\theta}}{\partial x_j} v_k \\ &= \frac{\partial}{\partial x_j} (\bar{\omega}_i v_j - v_i \bar{\omega}_j) + \bar{\omega}_i \bar{\theta} + \epsilon_{ijk} \frac{\partial \bar{\theta}}{\partial x_j} v_k, \end{aligned} \quad (\text{B3})$$

where $\boldsymbol{\omega} = \nabla \times \boldsymbol{v}$, and $\theta = \nabla \cdot \boldsymbol{v}$. Similarly, the tensor operation of the second term of the SGS stress involved in the first term can be written as follows:

$$\begin{aligned}
 \epsilon_{ijk} \frac{\partial}{\partial x_j} \left[\frac{\partial}{\partial x_m} (w_k w_m) \right] &= \epsilon_{ijk} \frac{\partial}{\partial x_j} \left(w_m \frac{\partial w_k}{\partial x_m} + w_k \frac{\partial w_m}{\partial x_k} \right) \\
 &= \epsilon_{ijk} \frac{\partial}{\partial x_j} \left[\epsilon_{kmn} \overline{\omega}_m w_n + \frac{\partial}{\partial x_k} \left(\frac{1}{2} w_m w_m \right) + w_k \frac{\partial w_m}{\partial x_m} \right] \\
 &= w_j \frac{\partial \overline{\omega}_i}{\partial x_j} - \overline{\omega}_j \frac{\partial w_i}{\partial x_j} + 2\overline{\omega}_i \vartheta + \epsilon_{ijk} \frac{\partial \vartheta}{\partial x_j} w_k \\
 &= \frac{\partial}{\partial x_j} (\overline{\omega}_i w_j - w_i \overline{\omega}_j) + \overline{\omega}_i \vartheta + \epsilon_{ijk} \frac{\partial \vartheta}{\partial x_j} w_k,
 \end{aligned} \tag{B4}$$

where $\boldsymbol{\omega} = \nabla \times \boldsymbol{v}$, and $\vartheta = \nabla \cdot \boldsymbol{v}$. Hence, the SGS term involved in the first term can be obtained as follows:

$$\begin{aligned}
 \epsilon_{ijk} \frac{\partial}{\partial x_j} \left[\frac{\partial}{\partial x_m} (\overline{v_k v_m} - w_k w_m) \right] &= \frac{\partial}{\partial x_j} [(\overline{\omega}_i v_j - \overline{\omega}_i w_j) - (\overline{v_i v_j} - w_i w_j)] \\
 &\quad + \overline{\omega}_i \theta - \overline{\omega}_i \vartheta + \epsilon_{ijk} \frac{\partial \theta}{\partial x_j} v_k - \epsilon_{ijk} \frac{\partial \vartheta}{\partial x_j} w_k.
 \end{aligned} \tag{B5}$$

We define $\Upsilon_{ij} = (\overline{\omega}_i v_j - \overline{\omega}_i w_j) - (\overline{v_i v_j} - w_i w_j)$. It is an antisymmetric tensor and is similar to the form in incompressible turbulent flows [56].

APPENDIX C: THE IDENTICAL RELATIONSHIPS OF THE PRESSURE TERMS AND THE REDUCED FORM OF THE VISCOSITY TERMS IN INCOMPRESSIBLE TURBULENT FLOWS

Under the constant-density hypothesis, Eq. (22) can be simplified as follows:

$$\Phi_i^1 = 0, \quad \Phi_i^2 = 0. \tag{C1}$$

Equation (23) can also be simplified as follows:

$$\overline{D}^1 = -\nu \left(\frac{\partial \overline{u}_i}{\partial x_j} + \frac{\partial \overline{u}_j}{\partial x_i} \right) \frac{\partial \overline{\omega}_i}{\partial x_j}, \quad \overline{D}^2 = -\nu \epsilon_{ikl} \frac{\partial}{\partial x_k} \left(\frac{\partial \overline{u}_i}{\partial x_j} + \frac{\partial \overline{u}_j}{\partial x_i} \right) \frac{\partial \overline{u}_i}{\partial x_j}. \tag{C2}$$

Here $\nu = \mu/\rho$ is the kinematic viscosity coefficient, and the dynamic viscosity coefficient μ is also assumed to be constant. Under the hypothesis of constant density, the Favre filter can be reduced to other direct filters, and we replace the symbol $\tilde{\cdot}$ with the symbol $\bar{\cdot}$ in the above derivation. The velocity gradient tensor and vorticity gradient tensor can be decomposed as follows:

$$\frac{\partial \overline{u}_i}{\partial x_j} = \overline{S}_{ij} + \overline{Q}_{ij}, \quad \frac{\partial \overline{\omega}_i}{\partial x_j} = \overline{R}_{ij} + \overline{\Xi}_{ij}. \tag{C3}$$

Here $\overline{S}_{ij} = (\partial \overline{u}_i / \partial x_j + \partial \overline{u}_j / \partial x_i) / 2$ is the symmetric component of the velocity gradient tensor, $\overline{Q}_{ij} = (\partial \overline{u}_i / \partial x_j - \partial \overline{u}_j / \partial x_i) / 2$ is the antisymmetric component of the velocity gradient tensor, $\overline{R}_{ij} = (\partial \overline{\omega}_i / \partial x_j + \partial \overline{\omega}_j / \partial x_i) / 2$ is the symmetric component of the vorticity gradient tensor, and $\overline{\Xi}_{ij} = (\partial \overline{\omega}_i / \partial x_j - \partial \overline{\omega}_j / \partial x_i) / 2$ is the antisymmetric component of the vorticity gradient tensor. Substituting the symmetric and antisymmetric components of the velocity and vorticity gradient tensors into Eq. (C2), the first and second viscous terms can be further simplified as follows:

$$\overline{D}^1 = -2\nu \overline{S}_{ij} \overline{R}_{ij}, \quad \overline{D}^2 = -2\nu \overline{R}_{ij} \overline{S}_{ij}. \tag{C4}$$

The simplified viscous terms are consistent with our previous work in the area of incompressible turbulent flows [56]. To conclude, the dual-channel characteristics of the pressure and viscosity terms exist only in compressible turbulent flows.

In compressible turbulent flows, the first and second channels of the pressure terms of helicity transfer are the same, except for spatial transportation. Hence, the pressure term of helicity transfer can be regarded as being twice as much as the first term [7]. In the following, we prove the identical relation of the dual channels of pressure terms.

First, we define the difference between the first and second channels of the pressure terms as Θ . If the first and second channels of the pressure terms are the same, Θ should be equal to zero:

$$\begin{aligned}\Theta &= -\frac{1}{\bar{\rho}} \frac{\partial \bar{p}}{\partial x_i} \epsilon_{ijk} \frac{\partial \tilde{u}_k}{\partial x_j} - \epsilon_{ijk} \frac{\partial}{\partial x_j} \left(-\frac{1}{\bar{\rho}} \frac{\partial \bar{p}}{\partial x_k} \right) \tilde{u}_i \\ &= -\frac{\partial \bar{p}}{\partial x_i} \left[\frac{1}{\bar{\rho}} \epsilon_{ijk} \frac{\partial \tilde{u}_k}{\partial x_j} - \epsilon_{ijk} \tilde{u}_j \frac{\partial}{\partial x_k} \left(\frac{1}{\bar{\rho}} \right) \right] \\ &= -\left[\frac{\partial}{\partial x_i} \left(\bar{p} \epsilon_{ijk} \frac{\partial (\tilde{u}_k / \bar{\rho})}{\partial x_j} \right) - \bar{p} \frac{\partial}{\partial x_i} \left(\epsilon_{ijk} \frac{\partial (\tilde{u}_k / \bar{\rho})}{\partial x_j} \right) \right].\end{aligned}\quad (\text{C5})$$

The first term on the r.h.s. of Eq. (C5) can be regarded as spatial transportation, and we focus on the second term. According to vector identity, we can obtain the following result:

$$\frac{\partial}{\partial x_i} \left(\epsilon_{ijk} \frac{\partial (\tilde{u}_k / \bar{\rho})}{\partial x_j} \right) = 0. \quad (\text{C6})$$

Hence, the first and second channels of the pressure terms are the same without considering spatial transportation.

-
- [1] B. A. Khesin and Y. V. Chekanov, Invariants of the Euler equations for ideal or barotropic hydrodynamics and superconductivity in D dimensions, *Physica D* **40**, 119 (1989).
 - [2] J. Z. Wu, H. Y. Ma, and M. D. Zhou, *Vorticity and Vortex Dynamics* (Springer, Berlin, 2006).
 - [3] D. Serre, Helicity and other conservation laws in perfect fluid motion, *C. R. Mec.* **346**, 175 (2018).
 - [4] J. J. Moreau, Constantes d'un îlot tourbillonnaire en fluid parfait barotrope, *C. R. hebd. séances Acad. sci. Paris* **252**, 2810 (1961).
 - [5] H. K. Moffatt and A. Tsinober, Helicity in laminar and turbulence flow, *Annu. Rev. Fluid Mech.* **24**, 281 (1992).
 - [6] T. B. Gatski and J. P. Bonnet, *Compressibility, Turbulence and High Speed Flow* (Academic Press, San Diego, CA, 2013).
 - [7] Z. Yan, X. Li, J. Wang, and C. Yu, Effect of pressure on joint cascade of kinetic energy and helicity in compressible helical turbulence, *Phys. Rev. E* **99**, 033114 (2019).
 - [8] H. K. Moffatt, Degree of knottedness of tangled vortex lines, *J. Fluid Mech.* **35**, 117 (1969).
 - [9] H. K. Moffatt, Helicity and singular structures in fluid dynamics, *Proc. Natl. Acad. Sci. USA* **111**, 3663 (2014).
 - [10] M. W. Scheeler, D. Kleckner, D. Promentb, G. L. Kindlmann, and W. T. M. Irvine, Helicity conservation by flow across scales in reconnecting vortex links and knots, *Proc. Natl. Acad. Sci. USA* **111**, 15350 (2014).
 - [11] M. W. Scheeler, W. M. van Rees, H. Kedia, D. Kleckner, and W. T. M. Irvine, Complete measurement of helicity and its dynamics in vortex tubes, *Science* **357**, 487 (2017).
 - [12] A. Brissaud, U. Frisch, J. Leorat, M. Lesieur, and A. Mazure, Helicity cascades in fully developed isotropic turbulence, *Phys. Fluids* **16**, 1366 (1973).
 - [13] V. Borue and S. A. Orszag, Spectra in helical three-dimensional homogeneous isotropic turbulence, *Phys. Rev. E* **55**, 7005 (1997).
 - [14] E. Jurčišinová, M. Jurčišin, and R. Remecký, Influence of helicity on the Kolmogorov regime in fully developed turbulence, *Phys. Rev. E* **79**, 046319 (2009).

- [15] L. Shtilman and W. Polifke, On the mechanism of the reduction of nonlinearity in the incompressible Navier–Stokes equation, *Phys. Fluids* **1**, 778 (1989).
- [16] A. Tsinober, M. Ortenberg, and L. Shtilman, On depression of nonlinearity in turbulence, *Phys. Fluids* **11**, 2291 (1999).
- [17] W. J. T. Bos and R. Rubinstein, On the strength of the nonlinearity in isotropic turbulence, *J. Fluid Mech.* **733**, 158 (2013).
- [18] M. Linkmann, Effects of helicity on dissipation in homogeneous box turbulence, *J. Fluid Mech.* **856**, 79 (2018).
- [19] Z. Yan, X. Li, Y. Fu, and C. Yu, The effect of helicity on kinetic energy cascade in compressible helical turbulence, *Adv. Appl. Math. Mech.* **11**, 700 (2019).
- [20] T. Teitelbaum and P. D. Mininni, Effect of helicity and rotation on the free decay of turbulent flows, *Phys. Rev. Lett.* **103**, 014501 (2009).
- [21] L. Biferale, S. Musacchio, and F. Toschi, Inverse energy cascade in three-dimensional isotropic turbulence, *Phys. Rev. Lett.* **108**, 164501 (2012).
- [22] L. Biferale, S. Musacchio, and F. Toschi, Split energy–helicity cascades in three-dimensional homogeneous and isotropic turbulence, *J. Fluid Mech.* **730**, 309 (2013).
- [23] G. Sahoo, A. Alexakis, and L. Biferale, Discontinuous transition from direct to inverse cascade in three-dimensional turbulence, *Phys. Rev. Lett.* **118**, 164501 (2017).
- [24] A. Alexakis, Helically decomposed turbulence, *J. Fluid Mech.* **812**, 752 (2017).
- [25] A. Alexakis and L. Biferale, Cascades and transitions in turbulent flows, *Phys. Rep.* **767-769**, 1 (2018).
- [26] F. Plunian, A. Teimurazov, R. Stepanov, and M. K. Verma, Inverse cascade of energy in helical turbulence, *J. Fluid Mech.* **895**, A13 (2020).
- [27] D. K. Lilly, The structure, energetics and propagation of rotating convective storms. Part II: Helicity and storm stabilization, *J. Atmos. Sci.* **43**, 126 (1986).
- [28] R. L. Thompson, C. M. Mead, and R. Edwards, Effective storm-relative helicity and bulk shear in supercell thunderstorm environments, *Weather Forecast* **22**, 102 (2007).
- [29] Y. Song and R. L. Lysak, Evaluation of twist helicity of flux transfer event flux tubes, *J. Geophys. Res.* **94**, 5273 (1989).
- [30] M. A. Berger, Rigorous new limits on magnetic helicity dissipation in the solar corona, *Geophys. Astrophys. Fluid Dyn.* **30**, 79 (1984).
- [31] A. M. Duquenne, P. Guiraud, and J. Bertrand, Swirl-induced improvement of turbulent mixing: Laser study in a jet-stirred tubular reactor, *Chem. Eng. Sci.* **48**, 3805 (1993).
- [32] Q. Nguyen and D. V. Papavassiliou, Using helicity to investigate scalar transport in wall turbulence, *Phys. Rev. Fluids* **5**, 062601(R) (2020).
- [33] Y. J. Dai, W. X. Huang, and C. X. Xu, Coherent structures in streamwise rotating channel flow, *Phys. Fluids* **31**, 021204 (2019).
- [34] Z. X. Yang and B. C. Wang, Capturing Taylor–Görtler vortices in a streamwise-rotating channel at very high rotation numbers, *J. Fluid Mech.* **838**, 658 (2018).
- [35] P. D. McCormack, H. Welker, and M. Kelleher, Taylor–Görtler vortices and their effect on heat transfer, *J. Heat Transfer* **92**, 101 (1970).
- [36] W. S. Saric, Görtler vortices, *Annu. Rev. Fluid Mech.* **26**, 379 (1994).
- [37] J. C. Andre and M. Lesieur, Influence of helicity on the evolution of isotropic turbulence at high Reynolds number, *J. Fluid Mech.* **81**, 187 (1977).
- [38] Q. Chen, S. Chen, and G. L. Eyink, The joint cascade of energy and helicity in three-dimensional turbulence, *Phys. Fluids* **15**, 361 (2003).
- [39] Q. Chen, S. Chen, G. L. Eyink, and D. D. Holm, Intermittency in the joint cascade of energy and helicity, *Phys. Rev. Lett.* **90**, 214503 (2003).
- [40] G. L. Eyink, Multi-scale gradient expansion of the turbulent stress tensor, *J. Fluid Mech.* **549**, 159 (2006).
- [41] J. Wang, Y. Yang, Y. Shi, Z. Xiao, X. T. He, and S. Chen, Cascade of kinetic energy in three-dimensional compressible turbulence, *Phys. Rev. Lett.* **110**, 214505 (2013).
- [42] G. L. Eyink and T. D. Drivas, Cascades and dissipative anomalies in compressible fluid turbulence, *Phys. Rev. X* **8**, 011022 (2018).

- [43] M. K. Verma, *Energy Transfers in Fluid Flows: Multiscale and Spectral Perspectives* (Cambridge University Press, Cambridge, 2019).
- [44] P. D. Ditlevsen and P. Giuliani, Cascades in helical turbulence, *Phys. Rev. E* **63**, 036304 (2001).
- [45] S. Kurien, M. A. Taylor, and T. Matsumoto, Cascade time scales for energy and helicity in homogeneous isotropic turbulence, *Phys. Rev. E* **69**, 066313 (2004).
- [46] G. Sahoo, F. Bonaccorso, and L. Biferale, Role of helicity for large- and small-scale turbulent fluctuations, *Phys. Rev. E* **92**, 051002(R) (2015).
- [47] G. Sahoo, M. De Pietro, and L. Biferale, Helicity statistics in homogeneous and isotropic turbulence and turbulence models, *Phys. Rev. Fluids* **2**, 024601 (2017).
- [48] F. Waleffe, The nature of triad interactions in homogeneous turbulence, *Phys. Fluids* **4**, 350 (1992).
- [49] M. Kessar, F. Plunian, R. Stepanov, and G. Balarac, Non-Kolmogorov cascade of helicity-driven turbulence, *Phys. Rev. E* **92**, 031004(R) (2015).
- [50] N. M. Rathmann and P. D. Ditlevsen, Role of helicity in triad interactions in three-dimensional turbulence investigated by a new shell model, *Phys. Rev. E* **94**, 033115 (2016).
- [51] J. Panickacheril John, D. A. Donzis, and K. R. Sreenivasan, Solenoidal scaling laws for compressible mixing, *Phys. Rev. Lett.* **123**, 224501 (2019).
- [52] M. Y. Reshetnyak, Effect of compressibility on the generation of hydrodynamic helicity in the earth's liquid core, *Geomagn. Aeron.* **52**, 398 (2012).
- [53] D. Kivotides and A. Leonard, Helicity spectra and topological dynamics of vortex links at high Reynolds numbers, *J. Fluid Mech.* **911**, A25 (2021).
- [54] T. Wu and W. J. T. Bos, Cascades of enstrophy and helicity in turbulence without vortex stretching, *Phys. Rev. Fluids* **7**, 094601 (2022).
- [55] Z. Yan, X. L. Li, C. P. Yu, and J. C. Wang, Cross-chirality transfer of kinetic energy and helicity in compressible helical turbulence, *Phys. Rev. Fluids* **5**, 084604 (2020).
- [56] Z. Yan, X. L. Li, C. P. Yu, J. C. Wang, and S. Y. Chen, Dual channels of helicity cascade in turbulent flows, *J. Fluid Mech.* **894**, R2 (2020).
- [57] J. Wang, L.-P. Wang, Z. Xiao, Y. Shi, and S. Chen, A hybrid numerical simulation of isotropic compressible turbulence, *J. Comput. Phys.* **229**, 5257 (2010).
- [58] J. Wang, M. Wan, S. Chen, and S. Chen, Kinetic energy transfer in compressible isotropic turbulence, *J. Fluid Mech.* **841**, 581 (2018).
- [59] W. Sutherland, The viscosity of gases and molecular force, *Philos. Mag. Ser.* **36**, 507 (1893).
- [60] R. Samtaney, D. I. Pullin, and B. Kosović, Direct numerical simulation of decaying compressible turbulence and shocklet statistics, *Phys. Fluids* **13**, 1415 (2001).
- [61] J. Wang, Y. Shi, L. P. Wang, Z. Xiao, X. T. He, and S. Chen, Effect of compressibility on the small-scale structures in isotropic turbulence, *J. Fluid Mech.* **713**, 588 (2012).
- [62] S. B. Pope, *Turbulent Flows* (Cambridge University Press, Cambridge, 2010).
- [63] H. Aluie, Scale decomposition in compressible turbulence, *Physica D* **247**, 54 (2013).
- [64] J. L. Yu and X. Y. Lu, Subgrid effects on the filtered velocity gradient dynamics in compressible turbulence, *J. Fluid Mech.* **892**, A24 (2020).
- [65] J. G. Ballouz and N. T. Ouellette, Tensor geometry in the turbulent cascade, *J. Fluid Mech.* **835**, 1048 (2018).
- [66] J. G. Ballouz and N. T. Ouellette, Geometric constraints on energy transfer in the turbulent cascade, *Phys. Rev. Fluids* **5**, 034603 (2020).
- [67] J. G. Ballouz, P. L. Johnson, and N. T. Ouellette, Temporal dynamics of the alignment of the turbulent stress and strain rate, *Phys. Rev. Fluids* **5**, 114606 (2020).
- [68] J. G. Ballouz, On the efficiency of the turbulent cascade, Ph.D. thesis, Stanford University (2020).
- [69] H. Aluie, Compressible turbulence: The cascade and its locality, *Phys. Rev. Lett.* **106**, 174502 (2011).
- [70] H. Aluie, S. Li, and H. Li, Conservative cascade of kinetic energy in compressible turbulence, *Astrophys. J.* **751**, L29 (2012).
- [71] P. K. Yeung, X. M. Zhai, and K. R. Sreenivasan, Extreme events in computational turbulence, *Proc. Natl. Acad. Sci. USA* **112**, 12633 (2015).
- [72] R. H. Kraichnan, On Kolmogorov's inertial-range theories, *J. Fluid Mech.* **62**, 305 (1974).

- [73] R. Benzi, S. Ciliberto, R. Tripicciono, C. Baudet, F. Massaioli, and S. Succi, Extended self-similarity in turbulent flows, *Phys. Rev. E* **48**, R29 (1993).
- [74] R. Benzi, L. Biferale, R. T. Fisher, L. P. Kadanoff, D. Q. Lamb, and F. Toschi, Intermittency and universality in fully developed inviscid and weakly compressible turbulent flows, *Phys. Rev. Lett.* **100**, 234503 (2008).
- [75] J. Wang, Y. Yang, Y. Shi, Z. Xiao, X. He, and S. Chen, Statistics and structures of pressure and density in compressible isotropic turbulence, *J. Turbul.* **14**, 21 (2013).
- [76] Y. Yang, J. Wang, Y. Shi, Z. Xiao, X. T. He, and S. Y. Chen, Intermittency caused by compressibility: A Lagrangian study, *J. Fluid Mech.* **786**, R6 (2016).
- [77] U. Frisch, *Turbulence: The Legacy of A. N. Kolmogorov* (Cambridge University Press, Cambridge, 1995).
- [78] M. S. Chong, A. E. Perry, and B. J. Cantwell, A general classification of three-dimensional flow fields, *Phys. Fluids* **2**, 765 (1990).
- [79] B. J. Cantwell, Exact solution of a restricted Euler equation for the velocity gradient tensor, *Phys. Fluids* **4**, 782 (1992).
- [80] M. Danish and C. Meneveau, Multiscale analysis of the invariants of the velocity gradient tensor in isotropic turbulence, *Phys. Rev. Fluids* **3**, 044604 (2018).
- [81] S. Goto, A physical mechanism of the energy cascade in homogeneous isotropic turbulence, *J. Fluid Mech.* **605**, 355 (2008).
- [82] D. Kuzzay, O. Alexandrova, and L. Matteini, Local approach to the study of energy transfers in incompressible magnetohydrodynamic turbulence, *Phys. Rev. E* **99**, 053202 (2019).
- [83] D. Block, I. Teliban, F. Greiner, and A. Piel, Prospects and limitations of conditional averaging, *Phys. Scr.* **T122**, 25 (2006).
- [84] S. Kida and M. Takaoka, Reconnection of vortex tubes, *Fluid Dyn. Res.* **3**, 257 (1988).
- [85] W. T. M. Irvine, Moreau's hydrodynamic helicity and the life of vortex knots and links, *C. R. Méc.* **346**, 170 (2018).
- [86] J. Yao and F. Hussain, A physical model of turbulence cascade via vortex reconnection sequence and avalanche, *J. Fluid Mech.* **883**, A51 (2020).
- [87] J. Yao, Y. Yang, and F. Hussain, Dynamics of a trefoil knotted vortex, *J. Fluid Mech.* **923**, A19 (2021).
- [88] D. Zhao and H. Aluie, Inviscid criterion for decomposing scales, *Phys. Rev. Fluids* **3**, 054603 (2018).
- [89] G. E. Elsinga, T. Ishihara, M. V. Goudar, C. B. da Silva, and J. C. R. Hunt, The scaling of straining motions in homogeneous isotropic turbulence, *J. Fluid Mech.* **829**, 31 (2017).
- [90] S. Khurshid, D. A. Donzis, and K. R. Sreenivasan, Energy spectrum in the dissipation range, *Phys. Rev. Fluids* **3**, 082601(R) (2018).
- [91] D. Buaria and K. R. Sreenivasan, Dissipation range of the energy spectrum in high Reynolds number turbulence, *Phys. Rev. Fluids* **5**, 092601(R) (2020).
- [92] H. Miura and S. Kida, Acoustic energy exchange in compressible turbulence, *Phys. Fluids* **7**, 1732 (1995).